PERFORMANCE OF CAVITATING AXIAL INDUCERS WITH VARYING TIP CLEARANCE AND SOLIDITY

Stanley Hammack Carpenter

PERFORMANCE OF CAVITATING AXIAL INDUCERS WITH VARYING TIP CLEARANCE AND SOLIDITY

71

Thesis by

Stanley Hammack Carpenter

Captain, United States Marine Corps

In Partial Fulfillment of the Requirements

For the Degree of

Aeronautical Engineer

California Institute of Technology

Pasadena, California

1957

ACKNOWLEDGEMENTS

The writer wishes to express his appreciation to Dr. A. J. Acosta, who not only initiated the research program, but whose interest, suggestions, and criticisms were instrumental in its completion.

The constant cooperation and many-faceted skills of Mr. Jack R. Kingan were invaluable in conducting the experiments.

Many thanks are extended to the remainder of the Hydrodynamics Laboratory staff for their assistance, as well as to Miss Helen Burrus of the Guggenheim Aeronautical Laboratory, who typed the manuscript.

ABSTRACT

The performance of a helical axial inducer pump was investigated in non-cavitating and heavily cavitating regimes over a wide range of tip clearance and solidity. It was found that cavity length is related to the occurrence of two cavitation phenomena: a non-steady or oscillating form of cavitation occurs when the cavity length is nearly equal to the spacing between the impeller blades, and complete pump failure is imminent if the cavity is nearly as long as the blade chord. The extent of the oscillating cavitation regime was little affected by the variation of tip clearance or solidity in the range investigated. However, an increase in tip clearance or a decrease in solidity definitely impairs cavitation performance at low inlet pressures. On the basis of these experiments a cavitation number limit is proposed for safe inducer operation.

TABLE OF CONTENTS

TABLE OF CONTENTS (Cont'd)

I. INTRODUCTION

The first successful rocket propulsion devices utilized solid propellants and were considered an ideal power source since there were no moving parts. However, since no reliable method of thrust variation for solid fuels has been developed, and the loading density is high, solid propellants are generally limited to short thrust-duration applications. Liquid propellants offer the advantages of variable thrust and higher specific impulse, but at the expense of added complexity and weight, since storage tanks, feed mechanisms, feed power supply, valves and associated hardware are required in addition to the thrust chamber. Various types of feed systems are available (Refs. 1 to 4), but for applications involving high thrust of long duration, overall propulsion system weight is minimized with a turbopump system. The unit utilizes a turbine to drive the pump, and its weight is not a strong function of duration.

To maintain their advantages, these turbopumps must be lightweight and compact, yet deliver a large volume of flow at a high pressure efficiently and reliably over a wide range of operating conditions. The impulse turbine is generally chosen as a power source because of its simplicity of construction, high-speed capability, light weight, and ability to withstand relatively high temperatures. Optimum turbine efficiency is governed by the ratio of the blade speed to the velocity of gas ejected by the nozzle, therefore the highest shaft speed and the largest turbine wheel diameter compatible with weight and structural considerations is desirable. Ideally, the pump should be mounted on the same shaft as the turbine

to eliminate gearing, but then pump design considerations will dictate shaft speed, due principally to the limitations imposed by cavitation.

Cavitation is a boiling phenomenon resulting when the local pressure becomes approximately equal to the vapor pressure of the working fluid. The initial effects of cavitation; i.e., noise, vibration, and the possibility of damage to pump parts, are followed by a throttling of pump throughflow due to the reduction of cross-sectional area (Refs. 2, 3, and 5). Serious consequences of such effects, especially the throttling, are easy to imagine in a hydraulically balanced system. Operating characteristics of pumps under cavitating conditions, then, are of primary importance in pump design and selection.

The choice of pump type will be dictated by the thrust required of the rocket motor, as the thrust generated is directly proportional to the mass flow rate of propellant. High discharge pressures are required of the pump to meet the demands of chamber inlet pressure plus injector pressure drop and losses in lines and valves. A centrifugal pump is capable of meeting these rather stringent requirements, but its usable operating range is severely limited by cavitation, since the head-flow rate curves of typical centrifugal pumps exhibit a rapid drop with the onset of cavitation (Refs. 2 and 3). A variety of workable solutions to the problem exist, such as addition of stages to the pump, gas pressurization, or over-design of components, but the added weight will generally offset the initial advantage of the turbopump. With the present state of the art, single-stage pumps are inadequate, but a "fix" for centrifugal

pump design deficiencies consists of the addition of an axial inducer or booster upstream of the main impeller.

Axial flow pump characteristics do not fall off sharply with the start of cavitation, and a head is produced well into the cavitating regime, although with reduced efficiency. Such an inducer can provide enough pressure at the inlet of the main pump to extend its usable operating range considerably. With proper design criteria available, it would be possible to choose an optimum inducer configuration which would minimize cavitation effects under a given set of operating conditions. Development of such criteria depends on knowledge of cavitation and its relationship to the internal flow. Flow patterns in rotating machinery are usually so complex, and the volume of experimental data on axial inducers so limited, that reliable design procedures do not exist at present.

From the above discussion, it is apparent that cavitation is the major limitation on axial inducer performance. Cavitation conditions are related to the cavitation number, a pressure coefficient similar to the familiar one of airfoil theory, except that the pressure difference of primary concern is between that in the free stream and that in the cavity. When used in conjunction with the occurrence of a deleterious cavitation phenomenon, a high cavitation number is indicative of poor performance; i.e., the phenomenon occurs at a higher value of inlet pressure or at a lower rotative speed. The minimum value of cavitation number at which an acceptable head rise can be maintained determines one boundary of the useful inducer operating range. An adequate mathematical

model for prediction of this value would be a most useful design tool. Unfortunately, the mathematical treatment of cavitation inception and cavity growth on the simplest of geometric shapes is so involved, that a precise three-dimensional theory is far from a reality and to date no such model, empirical or analytical, has been found. Although many have been proposed, the scarcity of experimental data and flow complexity render them inadequate for one or more of the following reasons:

(a) Cavity pressure is not, in general, the same as the vapor pressure of the working fluid

(b) Tip clearance effects are strong

(c) Real fluid effects may be quite important

(d) Three-dimensional flow effects are strong

(e) Non-steady flow conditions such as oscillating cavitation may occur.

Cavitation inception and cavitation performance of larger axial pumps have been studied in some datail by Acosta, Fuller, and Guinard (Ref. 5), while Rains (Ref. 6) investigated tip clearance flows. Helical inducer tests have been reported by Ross and Banerian (Ref. 7) and Nawoj (Ref. 8).

Nawoj's studies (Ref. 8) were the first to use the axial inducer test facility of the California Institute of Technology Hydrodynamics Laboratory. One of his most interesting discoveries was a regime of non-steady cavitation, in which the cavitation region shifts from one blade passage to another with a regular frequency dependent on flow-rate and suction pressure. The portion of the operating range

affected by this phenomenon was noticeably shifted by a change in tip clearance.

The next program in the test facility, then, was formulated with the objective of investigating performance of impellers of a different design over a wide range of tip clearances and solidities. This data would not only add to the body of axial inducer knowledge for design purposes, but permit further study of cavitation phenomena.

For the purpose of this work, the performance of such inducers is separated into three loose classifications; the non-cavitating overall head, flow rate, and efficiency curve, the distribution of total head and velocity behind the impeller, and finally, the overall performance under various conditions of cavitation. The performance of the machine is best presented in terms of dimensionless coefficients. These coefficients are the total head coefficient ψ , torque coefficient τ , flow coefficient ϕ, and the efficiency η. Appendix II defines these parameters and the specific quantities used to convert the pump head, power input, and volume flow rate into their respective dimensionless parameters. In these experiments, values of η represent the total head efficiency of the impeller alone and are, therefore, not to be compared with complete pump efficiencies.

The plan of presenting results is as follows: A characteristic curve for a typical impeller is presented and the effects of tip clearance and solidity are separately studied when no cavitation is present. A method of approximating the ϕ-ψ curve from simple theoretical

considerations is outlined and compared with the results. In the second category of performance results, the simple radial equilibrium theory (Ref. 9) is used to estimate the radial distribution of head and velocity for one impeller at two flow rates, and reasonably good agreement with test data is found. Then radial distribution of head for a typical impeller is examined at several flow rates ranging from 25 per cent above to 25 per cent below the best efficiency point. The way in which tip clearance and solidity affect this distribution is shown for two of these flow rates. The third and major area of interest is operation in a cavitating regime. Here the scaling parameters S (suction specific speed) and K (cavitation number) are determined for a typical impeller over the range of flow rates mentioned above, with a detailed examination of tip clearance and solidity effects at two flow rates. A report of visual observations of cavitation, accompanied by photographs, is presented, followed by a discussion of impeller breakdown, which sets forth a safe lower limit on the cavitation number for inducer operation.

II. EXPERIMENTAL PROGRAM

As mentioned in the previous section, Nawoj (Ref. 8) has done some experimental work on helical inducers. In his studies, a four-bladed impeller with a 12 degree tip angle was used. The function of the present work is to extend these observations and to explore the effects of tip clearance and solidity on cavitating and non-cavitating performance. Because of drive-motor power limitations, Nawoj could not obtain sufficiently high speed to investigate adequately the breakdown regime. For the present tests an impeller design was chosen that required less power so that higher speed and hence lower cavitation numbers could be obtained. The tip angle selected for this purpose was 9 degrees, and for manufacturing reasons three blades were chosen.

It should be mentioned here that the operating parameters; i.e., the values of ψ and ϕ, required for inducers as they are now used are considerably removed from conventional axial fan or pump practice. For this reason it is particularly important to obtain experimental data on the performance of such units, both in the non-cavitating and cavitating regimes. Of the pertinent design considerations, certainly the effects of tip clearance and solidity are among the most important.

In accordance with these ideas the following experimental program was outlined:

(a) Manufacture two 9 degree, three-bladed impellers, both with tip clearance ratio $\lambda = 0.0375$. One of these is to have a solidity of 2.5, and the other 3.25.

(b) Carry out complete performance tests on the impeller with a solidity of 2.5 at successively greater tip clearance ratios up to $\lambda = 0.50$.

The use of such high values of solidity; e.g., 2.5, as occurs in practice raises the question of whether they are really necessary, since the additional space required by a high solidity impeller complicates the bearing and critical shaft speed problem in most applications. Accordingly, for the last part of the program we have

(c) Select an optimum tip clearance, if such exists, and investigate the effect of solidities from 3.25 to 1.0.

Impeller details and tabulated values of pertinent dimensions are given in Fig. 1.

III. LABORATORY EQUIPMENT AND PROCEDURE

A. INTRODUCTION

The axial-flow pump facility used in these experiments was designed and built at the Hydrodynamics Laboratory, California Institute of Technology, for the purpose of investigating cavitation in high-speed axial inducers operating at low cavitation numbers, using water as a working fluid. Arrangement of the facility permits visual observation of the flow and determination of pump performance over a wide range of speeds, flow rates, and system ambient pressures. Features of the system are illustrated in Fig. 2.

B. PUMP AND HYDRAULIC CIRCUIT

The facility is essentially a simple closed hydraulic circuit consisting of a sixty-gallon storage tank, impeller test section and drive motor, and return pipe, shown in schematic in Fig. 3.

An entrance bell in the top of the storage tank discharges into the impeller working section, mounted on top of the tank. The impeller casing is lucite with an inside diameter of 2.000 in. at the time of manufacture, sealed at each end with 'O' rings to prevent leakage of air into or water out of the system. Two static pressure taps are provided 1.875 in. upstream of the impeller leading edge. Total head probes may be installed in either of two locations, one 0.375 in. upstream of the leading edge, the other 1.125 in. downstream of the trailing edge of the impeller.

A circular brass plate attached to the lucite casing at the entrance to the test section supports the lower shaft bearing spider, which consists of four sharp-edged brass struts of thin cross-

section. The spider supports a hemispherical brass fairing containing a bronze water-lubricated bearing.

The impeller shaft is 18-8 stainless steel, 1.000 in. in diameter, and is sectioned to permit rapid impeller changes.

The outlet diffuser and the drive motor are supported by a bracket with four legs extending to the tank top, so that the lucite casing bears no load except its own weight. The diffuser, manufactured in the Hydrodynamics Laboratory Machine Shop, directs the pump discharge into a horizontal 2-in. return pipe. The drive motor mounting plate mates with a facing on the diffuser top. A thrust bearing seat in the diffuser case serves to hold the thrust bearing and carbon ring shaft seal.

Return flow is measured by a flow-meter before reentering the main tank via a throttle valve. A commercial centrifugal pump can be connected to the system through a bypass line, providing means of obtaining additional flow in the circuit of up to ninety gallons per minute.

Dissolved air that has been removed from solution can be eliminated through several bleed lines tapped into the system at high points. The pressure level in the system is established by applying vaccum to a small reservoir with a free surface mounted above the facility.

A screen suspended from the tank top protects the working section from entrained solid particles. The head loss across the screen was measurable, but completely negligible for the purposes of these tests, being of the order of 0.01 feet of water at the highest flow rates and 0.001 feet of water at the lowest.

C. DRIVE MOTOR AND SPEED CONTROL

The history of the drive motor and the original calibration are discussed in detail in Reference 8, so only the salient features will be described here.

Impeller drive power is furnished by one end of a Dumore double-end, series-wound, 1/2 hp. motor, while the other end drives a selsyn generator through an 8:1 spur reduction gear.

Speed measurement is by comparison of the selsyn generator output with a constant-speed source, which is an integral part of the power-supply unit designed and built especially for the Hydrodynamics Laboratory. The constant-speed source may be varied between 1 and 999 rpm, in steps of 1 rpm. The total reduction from the motor is 12:1, made up of 8:1 between the inducer drive and the selsyn generator, and 3:2 between the selsyn receiver and the differential mechanism of the constant-speed source. Thus the motor speeds available for comparison are from 12 to 11, 996 rpm in 12-rpm steps. On- or off-speed indication is provided by a pointer on the control panel; adjustment to a null, or on-speed, indication is manually accomplished by varying the input power to the motor armature circuit.

Power input to the motor is measured with commercial types of voltmeter and ammeter, having an accuracy of two per cent at full deflection.

D. INSTRUMENTATION AND LIGHTING

Flow rate is measured with a propeller-type flow pick-up manufactured by the Waugh Engineering Company. The output signal of the meter is amplified, and pulses per second are counted by a Hewlett-Packard 522B electronic counter, and converted to volume rate of flow using the manufacturer's calibration data.

Total head is measured with a simple impact probe, 0.050 in. in diameter, connected to a water-mercury manometer which can be read to the nearest 0.01 in. Originally, the probe mount provided for radial traverse of the flow passage, using shims to determine radial distance. This was modified by attaching the probe to a traveling block, arranged so that distance can be measured in 0.009 in. steps, using a "click" device. Manometer connections include a valving system to prevent vapor cavity formation as system pressures are reduced with a vacuum pump.

A running-time meter reading in hours and tenths is used to maintain a record of impeller operating time while cavitating.

Impulses from a cam-actuated make-break contactor fire a General Radio Company Strobolux lighting unit through a trigger circuit. The actuating cam is located on the selsyn generator drive shaft, with a provision for phase rotation between contactor and cam lobe to permit observation of all blades at any peripheral station desired.

For still photography a 4x5 in. view camera is used in conjunction with two horizontally-opposed Edgerton type flash units. The flash duration is approximately 4 milliseconds, and both units

are fired simultaneously with camera shutter opening. For photographs of the upstream or suction blade surface, the camera was positioned with respect to an aerial camera periscope mirror.

An Eastman high-speed camera, exposing 3,000 frames per second, was used to photograph oscillating cavitation, lighted by two horizontally opposed banks of 3 photoflood lamps.

E. IMPELLERS

The basic inducer used in these tests has 3 blades, a hub ratio of 0.5, and a nominal diameter of 2.0 inches. The basic blade design is a rigid helix with a constant lead of 1.0 in.. The tip blade angle with respect to the plane of rotation is 9.04 degrees. Blade thickness varies from 0.040 in. at the tip to 0.035 in. at the hub. The material is 24 ST aluminum. Details of impeller design are shown in Fig. 1. Impellers were anodized for corrosion protection, but to save time between tests, surfaces machined to increase tip clearance or decrease solidity were simply coated with layout dye, which gave adequate protection for short immersion times.

F. PROCEDURE

The first step in obtaining experimental data is to eliminate as much dissolved air from the system as possible in a reasonable period of time. This is necessary to avoid foaming and entraining air bubbles in the circuit. An upper limit of 3.5 parts of air per million parts of water (on a molar basis) was set for the cavitation performance tests, and air content was measured with a Van Slyke Blood-Gas Analyzer. Steps in the preliminary procedure are:

1. Reduce system pressure as far as possible with the vacuum pump.
2. Operate inducer at a slow speed for several minutes, then stop and allow gas bubbles to accumulate near the top of the system.
3. Bleed off air bubbles, then adjust the level of the air-water interface.
4. Repeat process until the air content is at an acceptable level.
5. Purge manometer lines and check zeros.
6. Allow inducer to run for about 15 minutes to stabilize electrical and electronic components, then shut down and bleed all lines.
7. Record barometric pressure, air temperature and air content.
8. Bring inducer up to speed, then set the desired flow rate with the throttle valve.

Non-cavitating performance data for determination of characteristics was taken at 6000 rpm. This particular speed was chosen because speed scaling in the non-cavitating regime using the dimensionless parameters in this type of inducer is good (Ref. 8). The seal torque-absorption at this speed is more nearly constant, and cavitation, if any, is very limited in extent.

Data taken were the impeller total head measured midway between hub and case, and the power input to the drive motor as flow rate was varied, holding the speed constant and the inlet tank

pressure at an ambient pressure of 14.7 psia. From the impeller characteristic curves plotted from these data for the first impeller, flow coefficients were chosen for subsequent cavitation performance tests. The region of most interest is in the vicinity of the point of maximum efficiency, therefore the selected flow coefficients extend approximately 25 per cent above and below the best efficiency point. These values were fixed for subsequent cavitation tests. As it turned out, this was a fortunate choice, and the best efficiency points of all impellers lie within this zone.

Radial surveys of the non-cavitating total head at each of the selected flow coefficients were made at a speed of 9996 rpm. A later probe modification allowed measurement of the flow inclination (referred to the axial direction), static pressure, and total head for computation of the axial and whirl components of velocity downstream of the impeller.

The preliminary steps above are taken for cavitation tests, then the total head probe is checked for position at mid-passade and aligned with the flow. Readings are taken of the inlet tank pressure, total head downstream of the impeller, power input to the motor, and water temperature. Vacuum is then applied to the storage tank in increments of one to four inches of mercury, manometers are allowed to stabilize, the flow rate and speed checked, and readings taken. The larger increments of vacuum were used at the start of a particular flow rate test, then smaller steps were used as cavitation became more severe to provide more data points for better curves.

Visual observations of cavitation at each data point were translated into sketches or verbal description. Tank pressure was reduced until the maximum vacuum had been applied or until the inducer could no longer maintain the specified flow rate.

Upon completion of cavitation tests, a photographic survey of the cavitating regime for each impeller was made at two flow rates, to cover the following events (when possible), listed in order of decreasing inlet pressure:

1. Just prior to start of oscillating cavitation
2. Just after start of oscillating cavitation
3. Well-developed oscillating cavitation
4. Oscillation nearly stopped
5. Oscillation stopped, usually near breakdown.

IV. RESULTS AND DISCUSSION

A. INTRODUCTION

The results can be separated naturally into non-cavitating performance and cavitating performance, with the non-cavitating performance sub-divided into overall impeller characteristics and the more detailed internal flow surveys. The term "non-cavitating" performance is not strictly correct, since some cavitation was observed at all but the highest flow rates at the maximum inlet tank pressure. However, the effects of such cavitation are negligible compared to those observed during the cavitation tests.

In this section, one impeller (λ = 0.0375) has been chosen as typical of the series for presentation of a complete performance survey in each of the three divisions, impeller characteristics, radial total head distribution, and cavitating performance. Following examination of this data, effects of tip clearance and solidity on pertinent parameters is discussed. The dimensionless tip clearance λ (tip clearance/maximum blade thickness) was varied from 0.0375 to 0.500, while the solidity σ (chord/blade spacing) ranged from 3.25 to 1.0.

The velocity diagrams of Fig. 4 depict the physical flow relations.

B. IMPELLER CHARACTERISTICS (NON-CAVITATING)

1. Characteristics of a Typical Inducer (λ = 0.0375, σ = 2.5).

Impeller characteristics at λ = 0.0375 are shown in Fig. 5 with the head coefficient ψ , torque coefficient τ , and the efficiency

η as functions of the flow coefficient ϕ. The performance map compares favorably with inducers in use today (Ref. 7), and is typical of inducers tested. A theoretical head-flow curve derived from simple turning theory corrected for finite blade thickness and friction (Appendix I) is plotted for comparison. Slopes of the two curves are in good agreement at flow rates above $\phi = .090$, which is the range of most practical value. The large discrepancy at low values of ϕ is due in part to the tip clearance flow losses and the back-flow phenomenon reported by Nawoj (Ref. 8). Each of these effects is quite difficult to evaluate, but in the region of good efficiency (around $\phi = 0.09$) the approximation is considered adequate for preliminary design calculations.

It is particularly interesting to note here that the head curve is "stable" for all flow rates. That is, the head coefficient ψ is a continuously decreasing function of the flow coefficient ϕ. This behavior is to be contrasted with that of more conventional axial flow fans which exhibit a stall phenomenon with a sudden decrease in head coefficient as the flow rate is lowered. The fact that the inducer does not show such an effect is due to the very low blade angle and the strong radial flows that take place.

The torque coefficient, τ, shows the characteristic behavior of axial impellers with small blade angles. However, the numerical value may be several per cent in error due to variation in the torque absorbed by the impeller drive shaft seal (Section IV-E).

The efficiency η is also shown in Fig. 5 as a function of the flow coefficient, ϕ. The rather low value of maximum efficiency is

due primarily to the high solidity and to the low coefficient. (For a given lift-drag ratio the maximum efficiency, assuming no other losses, should occur near $\phi = 1.0$). The exact value of the efficiency is, of course, dependent upon the value of the seal drag, which is not constant. The seal drag, in addition to being non-constant, cannot be separated from the viscous drag of the impeller shaft. Therefore, tare measurements made with the impeller removed were arbitrarily adjusted for the decrease in the viscous drag of the impeller shaft when a favorable component of flow rotation is imparted to the pump discharge by the impeller. Therefore, for this impeller and for subsequent tests the magnitude of the efficiency and the trends observed will be correct. Moreover, the inducer efficiency is not a prime consideration in a complete pump, since it will require only about 10 per cent of the overall pump power input in a typical unit.

2. Effects of Tip Clearance.

As the tip clearance ratio, λ , is increased from 0.0375 through 0.1375, the head coefficient ψ (Fig. 6) does not change significantly, but further increase in λ leads to a decided decrease in slope and head coefficient, becoming more prounounced at the lower flow coefficients. Larger tip clearances produce higher leakage flow rates past the blade tip and the attendant decrease in total head and efficiency (Ref. 6), since the viscous forces in the gap are not strong enough to support the pressure differential between the upper and lower surfaces.

The torque coefficient variation with tip clearance is not large (Fig. 7). The curve for $\lambda = 0.0375$ is about 5 per cent below the mean value of the other curves, possibly due to a variation in seal torque absorption. Adjustment of this curve to the mean has no effect on the relative efficiency of this impeller, however.

The efficiency curves (Fig. 7) indicate a decided decrease with larger tip clearances. As mentioned previously, the measured efficiency may be somewhat in error, and although the efficiency is not to be disregarded, the actual numerical values are not considered critical in these tests. Therefore only the major trends are indicated. Figure 8 compares the maximum efficiency of impellers at each value of λ with Rains' theoretical curve for larger axial flow pumps (Ref. 6).

3. Effects of Solidity.

The effects of solidity in an impeller even with no cavitation is a subject all to itself, however, some of the gross effects are illustrated by these tests. The head and flow coefficient (ψ - ϕ) curves with decreasing solidity (Fig. 9) are similar in appearance to the curves for increasing tip clearance (Fig. 6), although the mechanism for the head change is quite different. Here the shorter blade chords cannot exert as much force on the fluid as can the longer blades, resulting in lower heads at comparable flow rates. No fluid loss is inherent in such a head decrease, however. The near coincidence of the curves for solidities of 3.25 and 2.5 indicates that nearly perfect guidance is being furnished the fluid, with the degree of guidance (and hence the head) decreasing as the

solidity is lowered. Even so, until the solidity becomes about 1.5 there is no significant change in the head produced at the flow rate for best efficiency. This result is to be expected since from simple cascade theory no appreciable change in the guiding effect occurs until the solidity is about 1.2. The differences that occur at low flow rates are probably due to a smaller amount of radial flow and/or backflow.

The efficiencies show a slight tendency to increase with lower solidity (Fig. 10). This trend should be expected, since from the consideration of friction alone, inducer efficiency at a solidity of 3.25 would not be as high as at a solidity of 2.0. The maximum efficiency obtained for each solidity is shown as a function of solidity in Fig. 11, illustrating the tendency to higher efficiency at the lower values of solidity.

It should be mentioned at this point that with one exception, each of the impellers tested for variable tip clearance or variable solidity was derived from a single impeller. Changes in λ or σ were obtained by machining so that in each case save one the same design was tested. The exception was an impeller of similar design but with a different leading edge shape, so that it is not precisely of the same series. This "irregular" impeller has a solidity of 2.5 and a dimensionless tip clearance of 0.1375, whereas the other impeller used in the solidity tests has a dimensionless tip clearance of 0.150, accounting for the irregularity of the point for $\sigma = 2.5$ in Fig. 11.

C. RADIAL HEAD DISTRIBUTION (NON-CAVITATING)

1. Radial Equilibrium.

In the overall performance tests reported thus far the total head was measured at the center of the passage about one-half diameter downstream of the impeller. It is known that a helical blade surface cannot impart a constant total head from hub to tip. As a result, the total head and the velocity are functions of the radius. A non-constant head distribution does not adversely affect the inducer efficiency of itself, but the axial and whirl components of the leaving velocity must be known if the following stage is to be correctly designed. A theoretical calculation of the dimensionless axial velocity ϕ_2, dimensionless whirl velocity C_u/U_o, and dimensionless head output ψ as functions of the radius ratio was made using the radial equilibrium theory of Reference 9. Measurements of the flow angle, total head, and static pressure were then made, using the impeller with $\lambda = 0.1375$, $\sigma = 2.5$. The observed and calculated data are compared in Figs. 12 and 13, for average flow coefficients of 0.093 and 0.087, respectively. Appendix I sets forth the manner in which the theoretical ψ and ϕ curves were obtained. The observed whirl velocity C_u/U_o multiplied by the radius ratio r/r_o is the measured dimensionless head input, ψ', at each radial station.

Several interesting observations are possible from the curves. The mean axial velocity occurs at a radius ratio of 0.72, so the error introduced by measuring total head at mid-passage (radius ratio 0.75) is small. The efficiency of the impeller is the ratio of measured head output to measured head input; i.e. ψ / ψ'. At mid-passage,

this figure is 78 per cent at $\phi = 0.093$ and 79.5 per cent at $\phi = 0.087$. Corresponding values taken from Fig. 7 are 68 per cent and 74 per cent respectively, indicating that the impeller efficiencies calculated from the motor input power may be low, but they are certainly of the right magnitude.

The actual curves deviate considerably from the theoretical, but with the complexity of the internal flow, the agreement is surprisingly good.

2. Radial Head Distribution in a Typical Inducer ($\lambda = 0.0375$, $\sigma = 2.5$).

Radial head surveys at seven values of flow coefficient ϕ (Fig. 14) obtained with a different impeller i.e., $\lambda = 0.0375$, $\sigma = 2.5$, are characteristic of the impellers tested. Flattening of the curves with increasing flow coefficient follows the pattern predicted by the radial equilibrium theory, with tip clearance flows and hub boundary layer effects probably accounting for the distortion near the casing and hub.

3. Effects of Tip Clearance.

In the course of these studies, the effects of tip clearance ratio and solidity were examined by testing each impeller configuration for its radial head distribution and cavitating performance at each of the values of flow coefficient for which radial surveys are shown in Fig. 14. However, the overall effects of tip clearance ratio and solidity are similar for all values of ϕ, though they are more pronounced as ϕ is decreased. Two values of ϕ were chosen

for illustrating these effects, one near the best efficiency (ϕ = 0.087) and one slightly higher (ϕ = 0.093), since these are in the range of most interest.

Radial head surveys at ϕ = 0.093 and ϕ = 0.087 are plotted in Fig. 15 for the various values of the dimensionless tip clearance, λ. The strongest effect noted is a general decline in head produced at the same flow rate as tip clearance is increased, accompanied by a slight flattening of the curve.

Curves for the λ = 0.1375 impeller depart from this pattern, with values of ψ considerably higher than at other values of λ. A portion of this deviation may be due to the small differences between this impeller and the one used for the other values of (See Section IV B3). Also, some four months elapsed between tests at λ = 0.1375 and the tests at other values. Similar runs were made to check the original data, and total heads were as much as 6 per cent lower. This is not excessive for the facility, so the original data is used.

4. Effects of Solidity

Solidity changes affect the radial head distribution as shown in Fig. 16. The higher head obtained at a solidity of 2.5 is also probably due to the differences between this impeller and the other as mentioned above. Otherwise, with lower solidity, lower heads are produced, and variation of the head with the radius ratio is much less.

D. CAVITATING PERFORMANCE

1. Introduction.

Pump performance in the cavitating regime is usually presented in terms of the suction specific speed S or the cavitation number K (Appendix II). Both of these parameters are dimensionless* coefficients and since they are related to each other either may be used as a similarity or modeling parameter. However the cavitation number K is more closely connected with the minimum pressure on the blade surface while S is more useful in applications, since it involves the operational quantities directly, i.e., shaft speed, flow rate, and the net position suction head. In this work, the cavitating performance is given in terms of K as well as S for convenience.

The values of S and K observed near "breakdown" are well out of the normal range of pump experience. For example, the maximum value of S recorded herein was about 35, 700, which corresponds to a value of K = 0.015, whereas the conventional "safe" limit for cavitation in pumps is about 8500 and the value of K is usually kept above 0.25 (Refs. 2 and 3). At the low values of cavitation number reached in these tests the fluid approaching the impeller is nearly at its boiling point and it is evident that substantial cavitation will take place in the runner. It is, of course, not desirable to design a machine for operation close to the breakdown condition because so little margin is left. It is necessary therefore

---

* It is realized that the suction specific speed S is dimensional in its customary form, lacking a factor of $(g)^{3/4}$. For brevity's sake it will be categorized as non-dimensional, since no confusion should arise in terrestrial applications.

to know the cavitating performance throughout the whole range from cavitation inception to breakdown, so that the pertinent regions of interest can be delineated. Moreover, it is necessary to know these as a function of the physical design variables; i.e., tip clearance, solidity, etc.

The plan of the preceding section is followed in describing the cavitating experiments; namely, complete cavitation data will be given for one impeller ($\lambda = 0.0375$, $\sigma = 2.5$). Then, for two selected flow rates, the effects of tip clearance and solidity will be shown. The subsequent discussion includes a verbal and pictorial description of the progress of cavitation from inception to breakdown. An empirical criterion for breakdown is then presented together with some remarks on the scaling of cavitation performance.

2. Cavitating Performance of a Typical Inducer ($\lambda = 0.0375$, $\sigma = 2.5$).

The head coefficient ψ as a function of cavitation number K for values of flow coefficient ϕ ranging from 0.067 to 0.107 is plotted in Fig. 17, and Fig. 18 is a similar plot of the suction specific speed S. In general, as the cavitation number decreases (or suction specific speed increases), the head drops gradually, with the flow coefficient being held constant. The decrease is quite gradual for the larger flow coefficients, but for the lower flow coefficients a sharp decrease is noted beginning at about K = 0.10. This decrease is observed to coincide with the beginning of "oscillating" cavitation, a non-steady form of cavitation described in a following section. It should be noted that none of these curves show data points at the completely

broken down condition. The points taken at the minimum K values were usually quite close to the breakdown, but due to circuit and speed control limitations it was not possible to obtain points after the impeller had failed.

In the case of a few flow coefficients, a slight head rise precedes impeller breakdown. This is believed to be due to a decrease in fluid friction as cavitation separates the fluid from the blade surface, as well as the cessation of the oscillating cavitation which usually occurs before breakdown.

The lowest value of K obtained with this impeller before breakdown occurred was 0.0147 and the maximum S was 35,650. In comparison, Nawoj (Ref. 8) reports a minimum K of 0.0187 and a maximum S of 24,400 with a 12 degree, four-bladed impeller. Oscillating cavitation was observed in the range indicated in Figs. 17 and 18. In this zone the cavitation was quite severe, as may be seen with reference to the photographs (Figs. 26 to 30).

3. Effects of Tip Clearance

The effects of tip clearance are shown in Fig. 19. It is evident that the tip clearance effects are not strong for a tip clearance ratio λ of less than 0.30. (It should be noted that the curve for $\lambda = 0.1375$ is from a different 9° impeller and is included for the sake of completeness). As λ increases beyond 0.30 the head begins to decrease rapidly, indicating that this value is about a maximum that should be used. The minimum value of K (or maximum value of S) did not depend too much on the tip clearance. However the least

value of K was found for λ = 0.10 at ϕ = 0.087 at which condition K = 0.019 and S = 31,750. Similar data are given for S in Fig. 20. In connection with Figs. 19 and 20, it should be mentioned that the impeller with tip clearance ratio λ = 0.30 was still somewhat removed from the "breakdown" point since system instabilities prevented observation at lower values of K.

Although moderate changes in tip clearance do not seem to effect the cavitation performance, two points remain to be discussed. The first of these is the pump efficiency and the second is the non-steady or oscillating cavitation. From the standpoint of efficiency it would appear that one would want to use the smallest tip clearance possible. This conclusion applies only to the non-cavitating regime, since efficiency could not be reliably measured in the fully cavitating zone. However, there seems to be little reason why this result should not be true here as well. Oscillating cavitation inception occurred at or near the points indicated in Figs. 19 and 20. The earliest inception was noted at the smallest tip clearance ratio tested (λ = 0.0375), and inception is delayed longest with λ = 0.1375. At other values of λ inception occurs approximately mid-way between these extremes, with tip clearance ratios larger than 0.20 having very little effect. However, the effect does not seem to be as large as might be indicated by Nawoj's experiments (Ref. 8). This point is taken up again in a following section.

There is no reason why oscillating cavitation should be avoided from the standpoint of hydraulic performance, but the remarks thus far imply that the zone of oscillating cavitation is to be avoided

at all cost. This is indeed the opinion of the writer, although it lacks confirmation through experience. Of course, one would like to suppress this effect for mechanical reasons; however, it may be that for many applications no problem exists. Certainly, this is a subject worthy of further study.

4. Effects of Solidity

In cavitating operation the function of the impeller is to provide a high pressure region in which cavities may be collapsed. As the solidity is decreased, the impeller cannot provide as much pressure for cavity collapse, and in addition there is less passage length for this process to occur. We expect therefore, that as the solidity decreases, the cavitation performance will deteriorate. This deterioration does in fact occur, principally as a head loss at all values of inlet pressure as the solidity is decreased (Figs. 21 and 22). Here, again, allowance is made for the non-conformity of the impeller with a solidity of 2.5. Two other effects are not evident from the figures, however. First, the cavitation number at pump breakdown shows a tendency to increase as the solidity is decreased, and will discussed in the next section. Second, the pump facility became unstable when it was operating in the range of suction specific speeds between 24,000 and 30,000, making data very hard to obtain. For the two flow rates presented, the highest suction specific speed, 29,550, and the lowest cavitation number, 0.0218, were obtained at a flow coefficient of 0.087 at a solidity of 2.5. Oscillating cavitation inception is only slightly affected by a change in solidity.

5. Impeller Breakdown

Considerable effort has been expended by various investigations in the search for a reliable breakdown criterion. One objective of the present program is to establish at least an empirical limit for breakdown. The term "impeller breakdown" is subject to a wide variety of interpretations. Here the term is used in the sense that at breakdown the impeller has ceased performing its functions almost entirely. Accordingly, the majority of data points termed "breakdown" should actually be identified as "at the verge of breakdown". The breakdown point itself is quite difficult to obtain, because once this limit is reached, impeller head and flow rate fall off rapidly toward zero, and the drive motor overspeeds with the sudden reduction in load. The higher of the cavitation numbers (hence, the lower specific speeds) plotted with the breakdown data fall into the category "not quite at breakdown", and this is taken into account in describing the usable impeller range.

Subject to the foregoing remarks, breakdown data are summarized in two fashions. In Figs. 23 and 24, breakdown values of cavitation number K and suction specific speed S are plotted as a function of tip clearance ratio λ and solidity σ, while Fig. 25 is a cross-plot of these same points with K as a function of flow coefficient ϕ. As mentioned previously (Section IV C3) cavitating performance tests were conducted at seven values of flow coefficient ϕ, and two of these values were utilized to exhibit the effects of tip clearance ratio and solidity. Figures 23, 24 and 25 summarize the

breakdown points observed at all values of flow coefficient ϕ for all impeller configurations.

From these figures it is seen that there is a definite tendency for the cavitation number at breakdown to increase with larger tip clearance (Fig. 23) and lower solidities (Fig. 24). The suction specific speed tends to decrease as tip clearance increases or as the solidity is lowered. An exact breakdown cavitation number cannot be assigned to a particular λ or σ, but the limit of operation can be defined as lying in a fairly narrow range of cavitation numbers. The width of this range is about 0.01 in K for varying λ, and about 0.005 in K for varying σ. Cavitation numbers at breakdown as a function of the flow coefficient ϕ, with varying λ and σ, are plotted in Fig. 25. Here, the scatter does not permit reliable curves to be drawn as functions of the variables λ and σ, although again a range of cavitation numbers in which breakdown is most likely to occur is evident.

The values of suction specific speed attained (Figs. 23 and 24), although high, are probably typical of such inducers. Ross and Banerian (Ref. 7), for example, indicate that even higher values (up to 65,000) can be obtained for a slightly different design. However, as will be pointed out later, there is the probability of considerable error in the measurement of cavity pressure at such conditions.

If the flow in the impeller is treated as a fully cavitating two-dimensional cascade by the method of Betz and Petersohn (Ref. 10 and Appendix I) the minimum cavitation number at breakdown (Fig. 25) is much too low. Of course this calculation neglects friction and

assumes irrotational motion, and should not therefore be expected to be a very accurate approximation. However, the majority of the breakdown points fall below twice the maximum cavitation number (for a given blade angle) obtained in this manner. This plot is shown in Fig. 25.

The validity of this rule was checked not only with the results of this program, but also with all available breakdown data in the Hydrodynamics Laboratory (largely unpublished) on 6, 9 and 12 degree blade angles. Only 6 points out of 93, or 6.5 per cent, were greater than twice the appropriate maximum K obtained in the manner indicated. Therefore, this approximation may be taken as a fairly reliable rule of thumb until better information becomes available.

6. Visual and Photographic Studies of Cavitation.

Some aspects of cavitation in this series of tests could not be measured quantitatively, therefore a narrative description accompanied by photographs will complete the picture of inducer operation. The sequence of events will be described in the direction of reduced inlet pressure, for operation at a constant speed. The development of cavitation is shown pictorially in Fig. 26.

The first visible cavity is a leading-edge separation cavity or bubble on the blade suction side. The cavity length is strongly dependent on flow rate, and the length increases from root to tip. Almost simultaneously a vortex cavity attached to the blade tip at the leading edge appears, with its axis aligned with the plane of rotation, and whose diameter increases as flow is throttled.

As inlet pressure is lowered, the dimension of the cavity increases, and the trailing edge becoming quite ragged (Figs. 26a and b). The tip clearance flow appears to follow the model proposed by Rains (Ref. 6); viz., a vortex sheet originating from the gap is rolled up by the free stream into a vortex on the suction side of the blade in which energy dissipation then takes place.

The first cavitation noise is heard as a low hum or buzz when the cavity length is of the order of one-fourth the blade spacing. Such noise is usually caused by bubble growth and collapse although noise from leading edge blade vibration may also take place.

At moderate cavitation numbers the separation cavity or blade surface cavitation extends from the hub to the blade tip, where it merges with the tip cavity. The surface of the separation cavity appears sheet-like and is generally steady until the tip cavity length approaches the blade spacing, s. At this point the cavity-water interface becomes wavy in appearance and increasingly unsteady near the cavity trailing edge. The unsteady portion of the cavity propagates toward the leading edge of the blade as lower cavitation numbers are reached. When the tip cavity length is almost equal to s, that is, as the cavity trailing edge nears the leading edge of the following blade (Fig. 26c), the cavitation is on the verge of oscillation. For each impeller tested, at every flow rate that produced oscillation, this rule held for the start of oscillation. Figure 27 shows the beginning of oscillating cavitation for the several values of λ tested. At $\lambda = 0.0375$, the trailing edge of the cavity has started to oscillate slightly, with the characteristic cloudy appearance as a portion of

the cavity collapses. At $\lambda = 0.1375$ the cavitation zone has spread into the following blade passage, but at other values of λ, we were fortunate enough to photograph the cavity nearer the actual start of oscillation.

With respect to one blade, oscillating cavitation appears as a sudden rapid growth of the cavity until it extends into the following blade passage, then an equally rapid shrinkage to a small fraction of the maximum size. As shrinkage is in progress on one blade, growth begins on another. Direction of rotation of these disturbances has not been determined but it appears to be the same as that of the impeller, but at a lower speed. This immediately suggests the rotating stall of axial compressors, and the possibility of a similar mechanism certainly exists.

The oscillation frequency has not been measured, but varies more or less directly with inlet pressure. In the present test set-up, oscillation-induced vibrations may be very severe, giving rise to the concern noted in a previous section. Still lower pressures aggravate the cavitation, which extends farther into blade passages on each oscillation cycle. At very low flow coefficients, back-flow takes place at the tip as observed by Nawoj (Ref. 8). Nearly axial vertical tip cavities can then extend upstream for some distance.

The oscillation generally ceases at some pressure before breakdown, and is signalled by a lower frequency and intensity of vibration. On cessation, more or less uniform cavities appear on all blades (Fig. 26d), with the tip cavity being indistinguishable from the blade surface cavity. As the cavity length approaches the blade chord

length, c, (Fig. 1) pump breakdown is imminent. Appearance of the cavitation near breakdown at $\phi = 0.074$ for various values of λ is shown in Fig. 28. In Fig. 29, appearance of the impeller with $\sigma = 1.0$ is shown near breakdown at two flow rates. The bubbling appearance of the blade surface cavity is shown in Fig. 30. This photograph is an oblique view taken through a mirror, so that the direction of rotation is to the observer's left, whereas in all other photographs rotation is to the right. At breakdown, impeller head and flow rate fall rapidly, and portions of the system are boiling, with bubbles appearing in the free stream ahead of the impeller (Fig. 26d).

A hysteresis effect on the stopping point of oscillating cavitation was also noted. That is, once the pump had broken down, if pressure in the system was gradually increased, oscillation would start at a higher pressure than that at which it stopped with pressure reduction.

The back flow predicted by the radial equilibrium formula was observed in tuft studies by Nawoj (Ref. 8), and is of the nature indicated in Fig. 29, where cavitation makes it visible.

As was mentioned previously (Section IV D3) an increase in tip clearance decreases the extent of the oscillating cavitation zone, as reported by Nawoj (Ref. 8), but investigation of the phenomenon over a wide range of tip clearance does not indicate a strong dependence of the zone extent on the tip clearance ratio. Variation of the solidity has an even smaller effect, although the intensity of the vibration and the noise is decreased at the lower solidities, probably due to the shorter blade chords.

The lack of a strong effect on oscillation by changing tip clearance and solidity is a disappointment in a way, since hope had been entertained of eliminating or at least considerably reducing the oscillation zone by varying these quantities.

One interesting observation was made, however, in that alternate blade cavitation observed by Nawoj (Ref. 8) on four-blade impellers did not occur on three-blade impellers. Preliminary tests on two-blade designs did reveal alternate-blade cavitation, but any conclusion as to the significance of these observations must await further tests.

7. Cavity Pressures

Pressure scaling of cavitation phenomena is accomplished with the cavitation number K. For most applications and in experimental work, the cavity pressure is usually assumed to be the vapor pressure of the fluid at stream temperature. Parkin and Kermeen (Ref. 11) in their experiments on cavitating hydrofoils in water, found that cavity pressure in general is higher than vapor pressure, enough higher to introduce serious errors into cavitation number calculations.

To gain some idea of the order of magnitude of the error introduced by assuming that cavity pressure is equal to the water vapor pressure, a few cavity pressures were measured in the impeller test section as follows: the impeller was removed, and a block constructed to restrict the pump passage to a known cross-sectional area. A thin sharp-edged tab perpendicular to the free stream was mounted immediately upstream of the total head probe.

Flow was started with the service pump and increased until a cavity was formed large enough to envelop the probe, and cavity pressure was measured with a differential manometer.

The pressures so measured in the cavity were at least 25 per cent higher than the vapor pressure of water, agreeing with similar measurements of Parkin and Kermeen (Ref. 11). However, this effect is no doubt dependent on the amount of supersaturation of the liquid with air. However, for the present tests the water entering the working section was always slightly supersaturated; so that the effect of air content could not be tested properly. Calculations assuming equilibrium air pressure in the cavity were also made and it is found that the cavity pressure so calculated is too high, and can even result in a negative cavitation number.

With the complexity of cavity pressure measurement (a subject all to itself) and a lack of a better scheme, computations for these data were made assuming a cavity pressure equal to the vapor pressure, with the reservation that the cavitation number so computed may be twenty-five per cent or so high. These results are indicative of the caution one must observe in applying breakdown cavitation results to different liquids. One should expect that the cavity size depends principally on the cavitation number (neglecting Reynolds number effects), but the cavity pressure can conceivably be greater or less than the equilibrium vapor pressure of the fluid.

V. SUMMARY AND CONCLUSIONS

Tests were conducted and extensive data were obtained on the internal flow distribution and cavitation performance of a helical inducer with a 9 degree tip blade angle over a wide range of tip clearance and solidity. Results show that such inducers form relatively efficient units at very high suction specific speeds and very low cavitation numbers. Hence, the data presented should be directly applicable to inducer design. The radial equilibrium theory is found to be fairly successful in calculating the downstream velocity profile, providing means of designing a subsequent stage.

Oscillating or non-steady cavitation was observed to start as the cavity length approached the blade spacing, s. The magnitude and extent of the oscillating cavitation regime is not markedly affected by changes in tip clearance ratio in the range from 0.0375 to 0.500, or by solidities ranging from 3.25 to 1.0.

Complete breakdown of the pump is imminent if the cavity is approximately as long as the blade chord. A simple empirical rule for determining a lower limit for safe inducer operation is proposed as being twice the maximum theoretical cavitation number computed for breakdown if the impeller is considered to be a fully cavitating two-dimensional cascade. The limit so established is higher than 93.5 per cent of the observed breakdown cavitation numbers, and much below the 'safe' limit used in axial pump practice today.

The question of adequate performance scaling of cavitation from one liquid to another or from one speed to another is still open. It is suggested that further work along these lines be undertaken.

REFERENCES

1. Sutton, G. P., Rocket Propulsion Elements, 2nd Edition, John Wiley and Sons, Inc. (1956).

2. Wislicenus, G. F., Fluid Mechanics of Turbomachinery, McGraw-Hill Book Co. (1947).

3. Stepanoff, A. J., Centrifugal and Axial Flow Pumps , John Wiley and Sons, Inc. (1948).

4. Shepherd, D. G., Principles of Turbomachinery, The MacMillan Co., (1956).

5. Guinard, P., Fuller, T., Acosta, A. J., "An Experimental Study of Axial Flow Pump Cavitation", Report E-19.3, (August 1954), Hydrodynamics Laboratory, California Institute of Technology.

6. Rains, Dean A., "Tip Clearance Flows in Axial Flow Compressors and Pumps", Report No. 5, (June 1954), Hydrodynamics Laboratory, California Institute of Technology.

7. Ross, C. C., and Banerian, G., "Some Aspects of High Suction Speed Inducers", Paper 55-A-124 read at ASME Diamond Jubilee Meeting, Chicago, Ill., (Nov. 1955).

8. Nawoj, Henry J., Cavitation Studies in Axial Inducers", Thesis for Aeronautical Engineer, California Institute of Technology, (1956).

9. Bowen, J. T., Sabersky, R. H., Rannie, W. D., "Theoretical and Experimental Investigations of Axial Flow Compressors", Summary Report under Navy Contract N6-ORI-102 Task Order IV, (June 1949), Mechanical Engineering Laboratory, California Institute of Technology.

10. Betz, A., and Petersohn, E., "Anwendung der Theorie der freien Strahlen", Ingenieour Archiv, Band II (1931).

11. Parkin, B. R., and Kermeen, R. W., "Water Tunnel Techniques for Force Measurements on Cavitating Hydrofoils", Journal of Ship Research, Vol. 1, No. 1, (April 1957).

APPENDIX I

A. APPROXIMATION OF THE HEAD-FLOW CURVE FROM SIMPLE TURNING THEORY.

If no blockage is assumed, the theoretical head coefficient at the root mean square hub ratio may be derived from the velocity diagram, Fig. 4, and the impeller geometry, Fig. 1, as

$$(1) \qquad \psi_{th} = \xi_m^2 \left(1 - \phi_o \cot \beta_o\right).$$

Blockage increases the effective flow rate through the impeller, so using 12 per cent blockage, this relation becomes

$$(2) \qquad \psi_{th} = \xi_m^2 \left(1 - 1.12\, \phi_o \cot \beta_o\right).$$

If a friction head loss of the form $H_f = \frac{f}{4} \frac{\ell}{R} \frac{V_1^2}{2g}$ is assumed, then the loss in head coefficient due to friction is

$$(3) \qquad \psi_f = \frac{H_f g}{U_o^2} = \frac{f}{8} \frac{\ell}{R} \left[1 + (1.12\, \phi_o)^2\right].$$

Here f is the friction factor for turbulent flow in smooth pipe with the Reynolds number based on the chord at the r.m.s. hub ratio and a mean relative velocity in the range of interest, ℓ is the blade chord length at the r.m.s. hub ratio, and R is the hydraulic radius of the passage normal to the flow.

The difference of equations 2 and 3 yields the equation of the theoretical head-flow curve plotted in Fig. 5.

B. RADIAL EQUILIBRIUM THEORY APPLIED TO A HELICAL INDUCER.

The radial equilibrium formula for a rotor, equation 12b of Reference 9, in the case of the axial inducer with axial inlet flow reduces to the simple form

$$(4) \qquad \phi_2(\xi) = \tan\beta_o - \frac{\cot^2\beta_o(\tan\beta_o - 1.12\,\phi_1)(1-\xi_i^2)}{(1+\xi^2\cot^2\beta_o)\,\ln\left(\frac{1+\cot^2\beta_o}{1+\xi_i^2\cot^2\beta_o}\right)}$$

where ϕ = average flow coefficient = $\frac{C_a}{U_o}$

and 1.12 = blockage ratio.

Since $C_u = r\omega - C_a \cot\beta_o$

$$(5) \qquad \frac{C_u}{U_2} = \xi\left(1 - \phi_2 \cot\beta_o\right), \qquad \text{and}$$

$$(6) \qquad \psi' = \xi\,\frac{C_u}{U_2} = \xi^2\left(1 - \phi_2\cot\beta_o\right).$$

Equations 4 and 6 are plotted in Figs. 12 and 13.

C. CAVITATING CASCADE BREAKDOWN APPROXIMATION.

If the inducer is treated as a cavitating two-dimensional cascade with no blockage (Ref. 10), the cavitation number when the cavity length is equal to the blade chord is given approximately (Ref. 8) by

$$K = \alpha\,\phi,$$

where K, α , and ϕ are local quantities. Rewriting this equation in terms of conditions at the r.m.s. hub ratio,

$$(7) \qquad K_m = \left(\frac{1+\phi_o^2}{\xi_m^2+\phi_o^2}\right)\left(\frac{\phi_o}{\xi_m}\right)\left(\beta_m - \frac{\phi_o}{\xi_m}\right).$$

Equation 7, plotted in Figure 25 for the impellers used in these tests, represents the theoretical cavitation number at which impeller breakdown will occur.

APPENDIX II

DEFINITIONS, NOTATION, AND SYMBOLS

Derivation of the non-dimensional hydraulic parameters and the scaling parameter, S, is extensively discussed in the literature (Refs. 2, 3, and 4), therefore only definitions and some derived relations are included here.

Notation included below is generally used throughout the report, and any deviations from this list are explained in the accompanying text.

A — flow passage cross-sectional area (ft.^{2})

C — axial component of velocity (ft./sec.)

H — hydraulic head, ft. of water

K — cavitation number = $\frac{p_1 - p_K}{\frac{1}{2}\rho V_1^2} = \frac{\frac{2(NPSH)g}{U_o^2} - \phi_o^2}{(1+\phi_o^2)}$

N — revolutions per minute

NPSH — net positive suction head = $H_s + H_a - H_v$

Q — volume rate of flow, (ft.^{3}/sec.)

R — hydraulic radius = area normal to flow/wetted perimeter

S — suction specific speed = $\frac{21.2\ N(Q)^{1/2}}{(NPSH)^{3/4}}$

T — torque

U — peripheral velocity (ft./sec.)

V — relative velocity (ft./sec.)

c — blade chord length (ft.)

g	gravitational acceleration, assumed constant and equal to 32.2 ft./sec.^{2}
h	blade thickness (ft.)
p	pressure (lb./ft.^{2})
r	radial distance (ft.)
r.m.s.	root mean square
s	blade spacing = impeller diameter/number of blades
z	axial extent of blades
α	angle of attack (radians)
β	blade angle measured from plane of rotation
δ_t	tip clearance
η	efficiency = $\phi_o \psi_o / \tau$
λ	dimensionless tip clearance = δ_t / h
ξ	radius ratio = r/r_o
ρ	density (slugs/ft.^{3})
σ	solidity = c/s
τ	dimensionless torque coefficient = $\dfrac{T}{\rho\, r_o U_o^2 A}$
ϕ	dimensionless flow coefficient = $\dfrac{Q}{A U_o}$
ψ	dimensionless head coefficient = $\dfrac{gH}{U_o^2}$
ω	angular velocity, radian/second

Subscripts:

0	impeller tip
1	far upstream of the impeller
2	far downstream of the impeller
a	atmospheric, or axial component of velocity
i	impeller hub
k	cavity
m	evaluated at the root mean square hub ratio
s	suction
u	whirl component of velocity
v	vapor

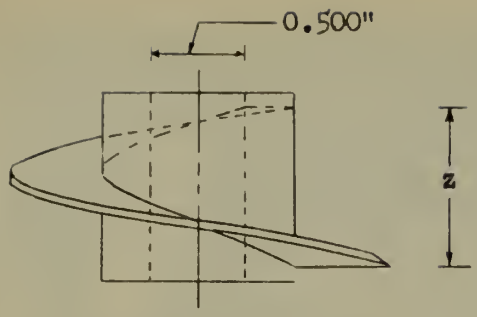

TYPICAL BLADE PROFILE

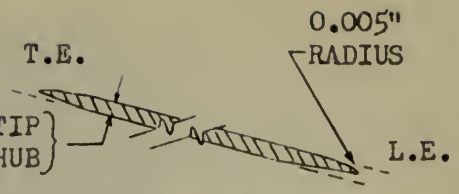

LEADING AND TRAILING EDGE FILING DETAIL

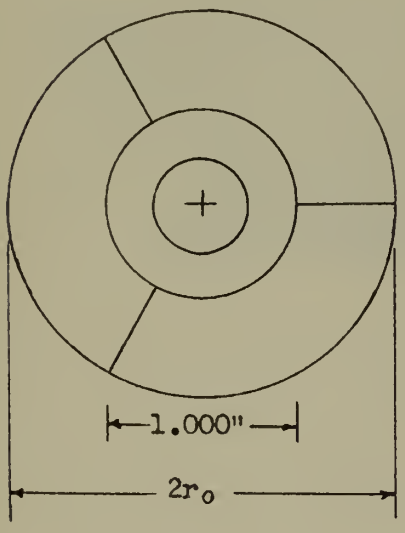

BOTTOM VIEW OF IMPELLER

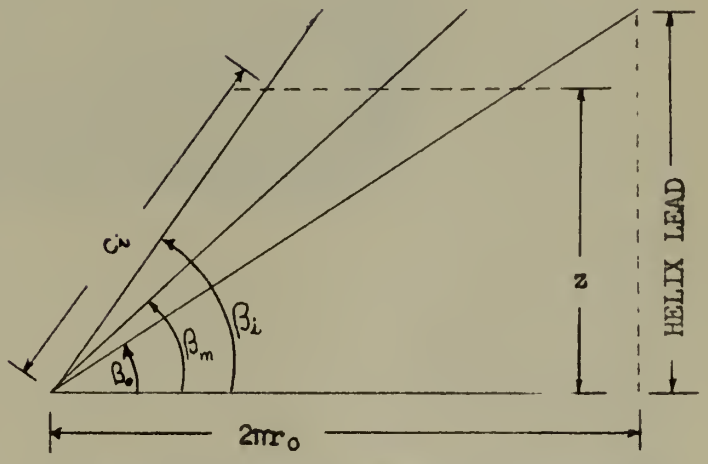

DEVELOPED HELIX GEOMETRIC RELATIONS

PRINCIPAL IMPELLER DIMENSIONS						
λ	σ	r_o (in.)	β_o (o)	c_0 (in.)	z (in.)	δ_t (in.)
.0375	2.5	1.000	9.04	5.28	.83	.0015
.100	2.5	.9975	9.06	5.27	.83	.0040
.1375	2.5	.9960	9.08	5.26	.83	.0055
.200	2.5	.9935	9.10	5.25	.83	.0080
.300	2.5	.9895	9.14	5.23	.83	.0120
.500	2.5	.9815	9.21	5.19	.83	.0200
.1500	3.25	.9955	9.08	6.78	1.07	.0060
.1500	2.0	.9955	9.08	4.17	.66	.0060
.1500	1.5	.9955	9.08	3.13	.49	.0060
.1500	1.0	.9955	9.08	2.09	.33	.0060

FIG. 1 IMPELLER DETAILS

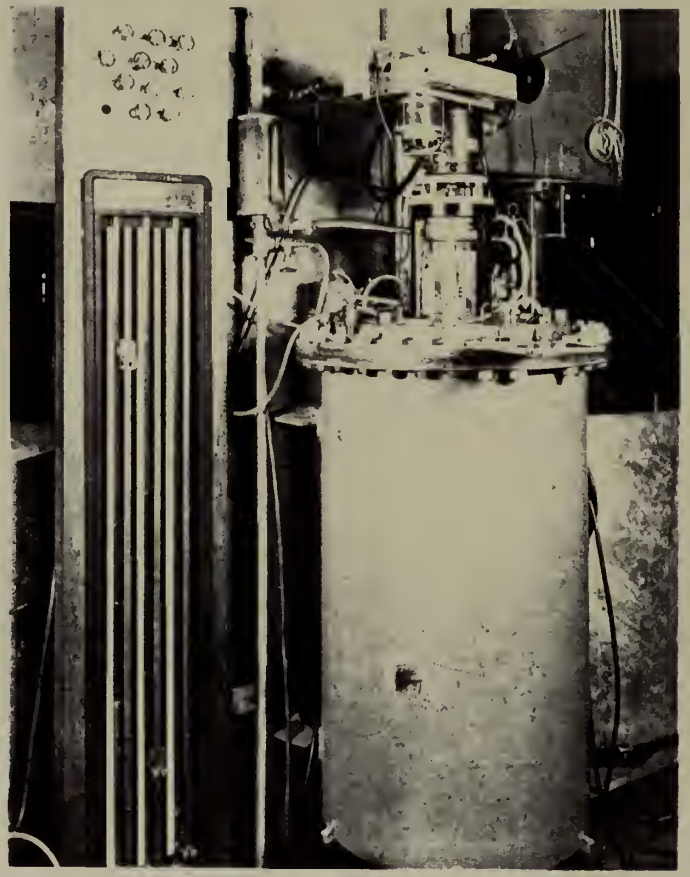

(a) Arrangement of facility

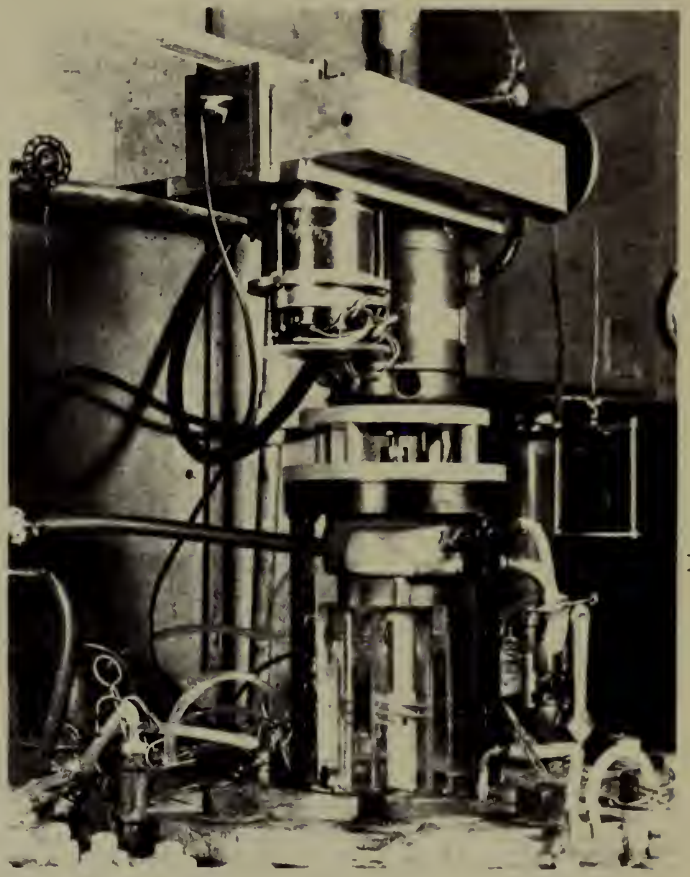

(b) Close-up of impeller test section

Fig. 2 Axial Inducer Test Facility

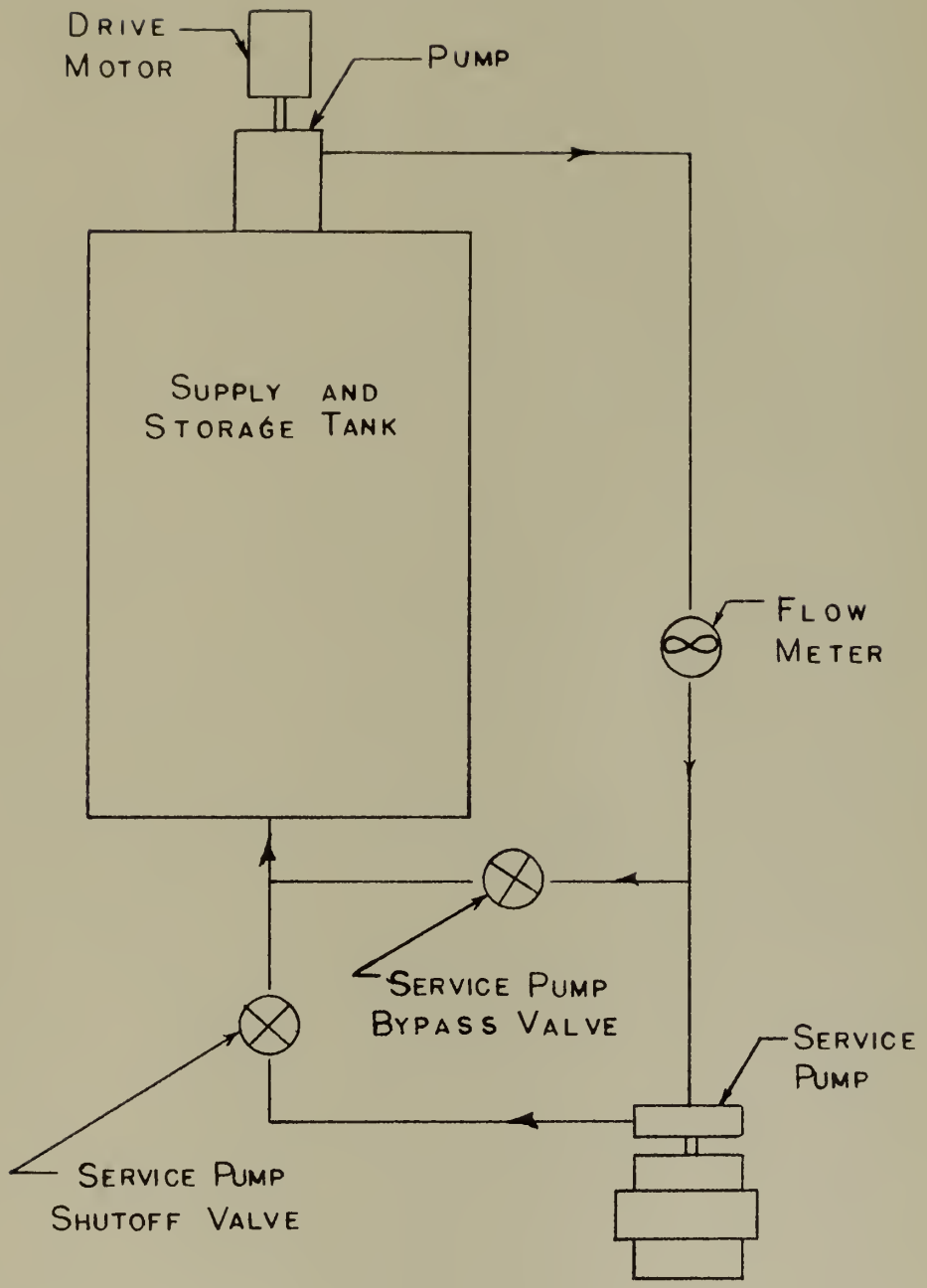

FIG. 3 HYDRAULIC CIRCUIT SCHEMATIC

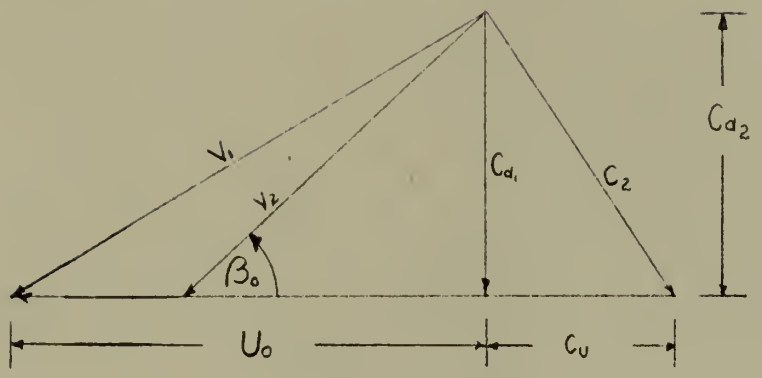

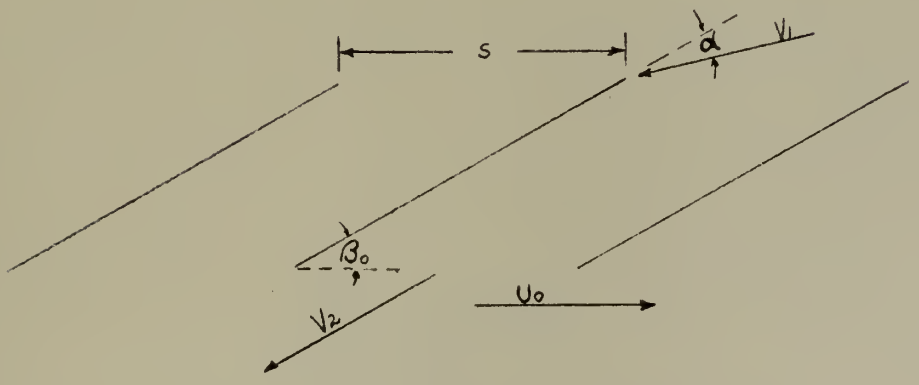

FIG. 4 VELOCITY DIAGRAMS FOR A NON-CAVITATING CASCADE

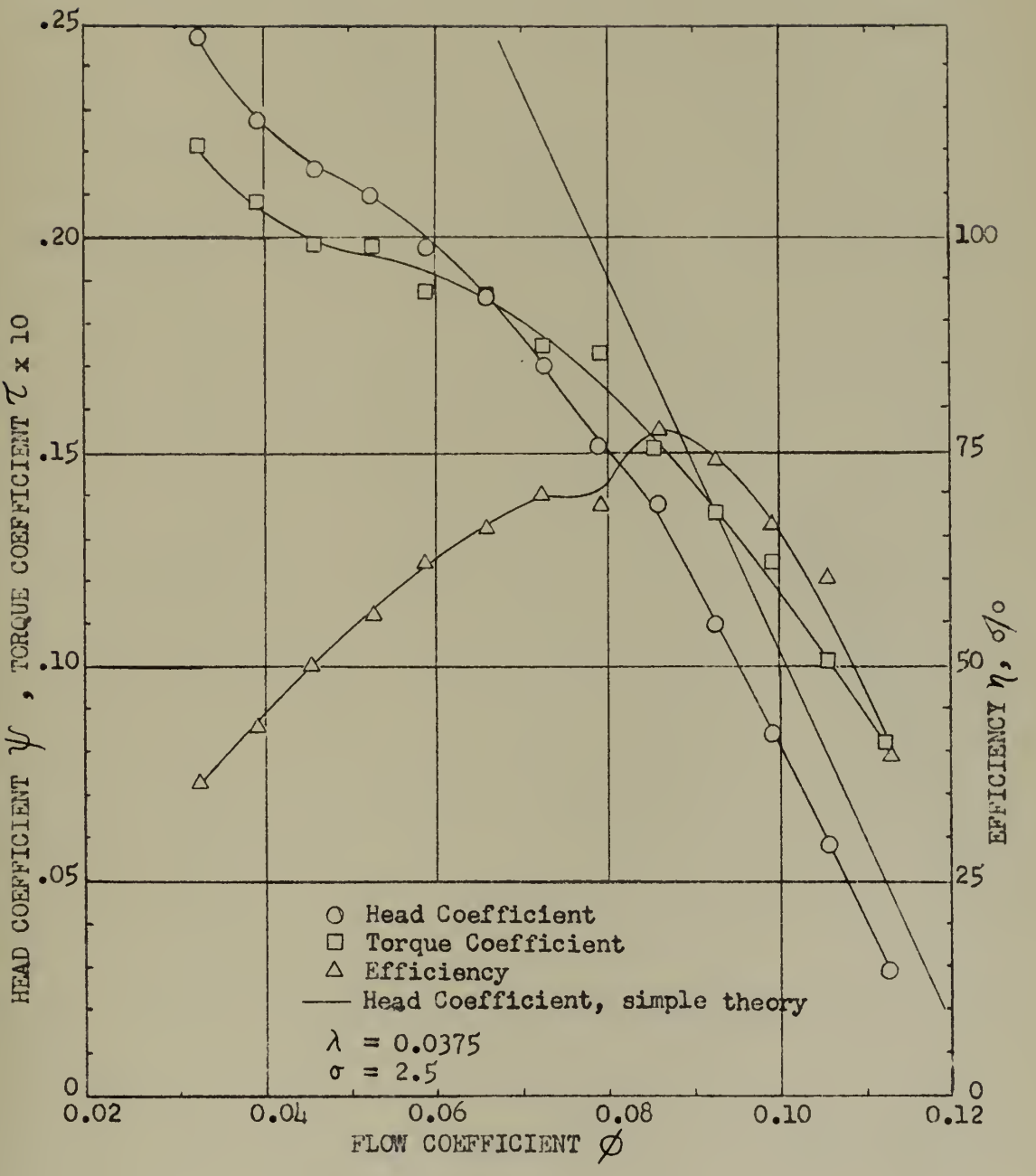

FIG. 5 TYPICAL IMPELLER CHARACTERISTICS (NON - CAVITATING) FOR A HELICAL 9 DEGREE IMPELLER

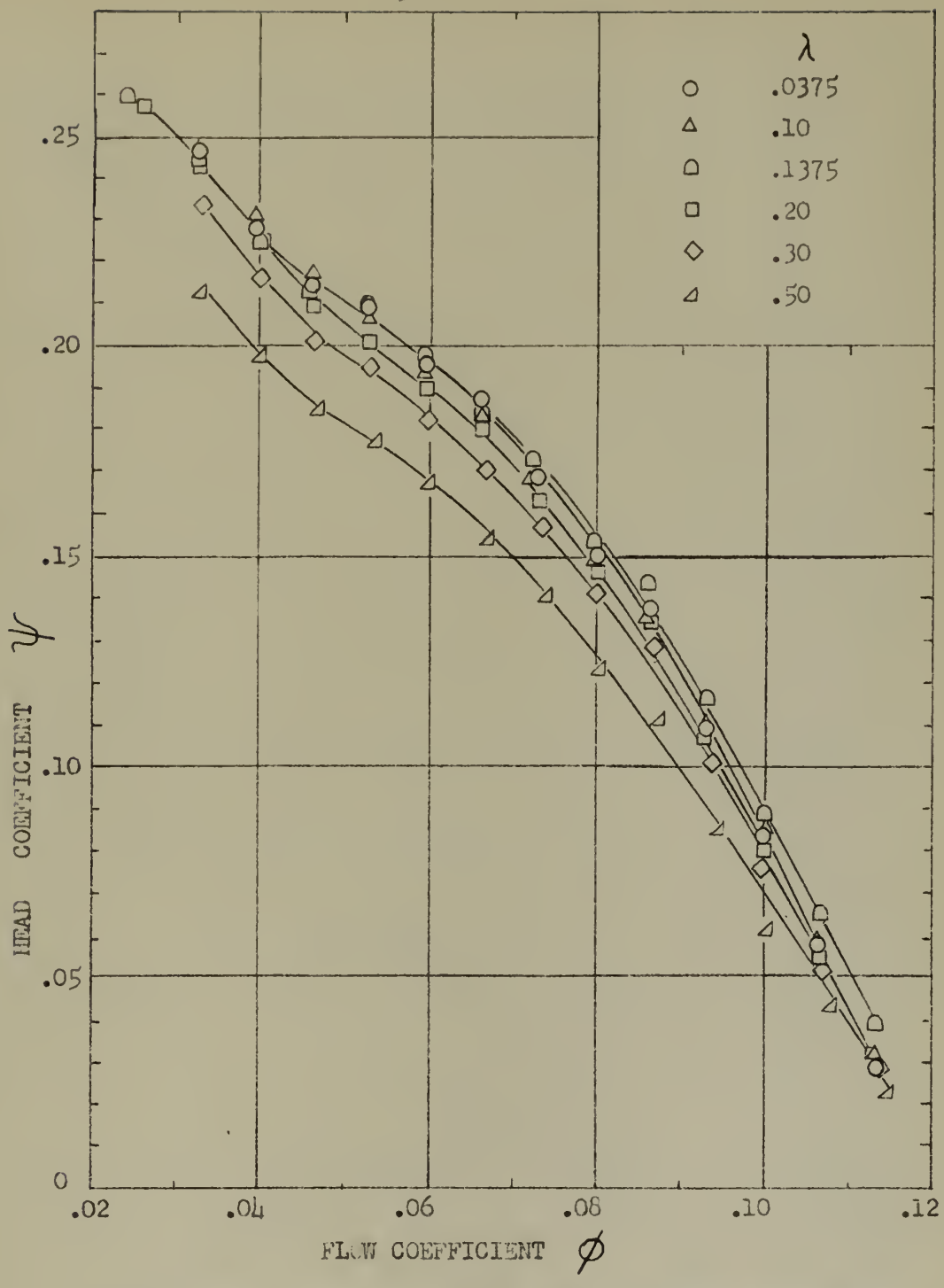

FIG. 6 HEAD COEFFICIENT vs. FLOW COEFFICIENT WITH VARYING TIP CLEARANCE RATIO, $\sigma = 2.5$

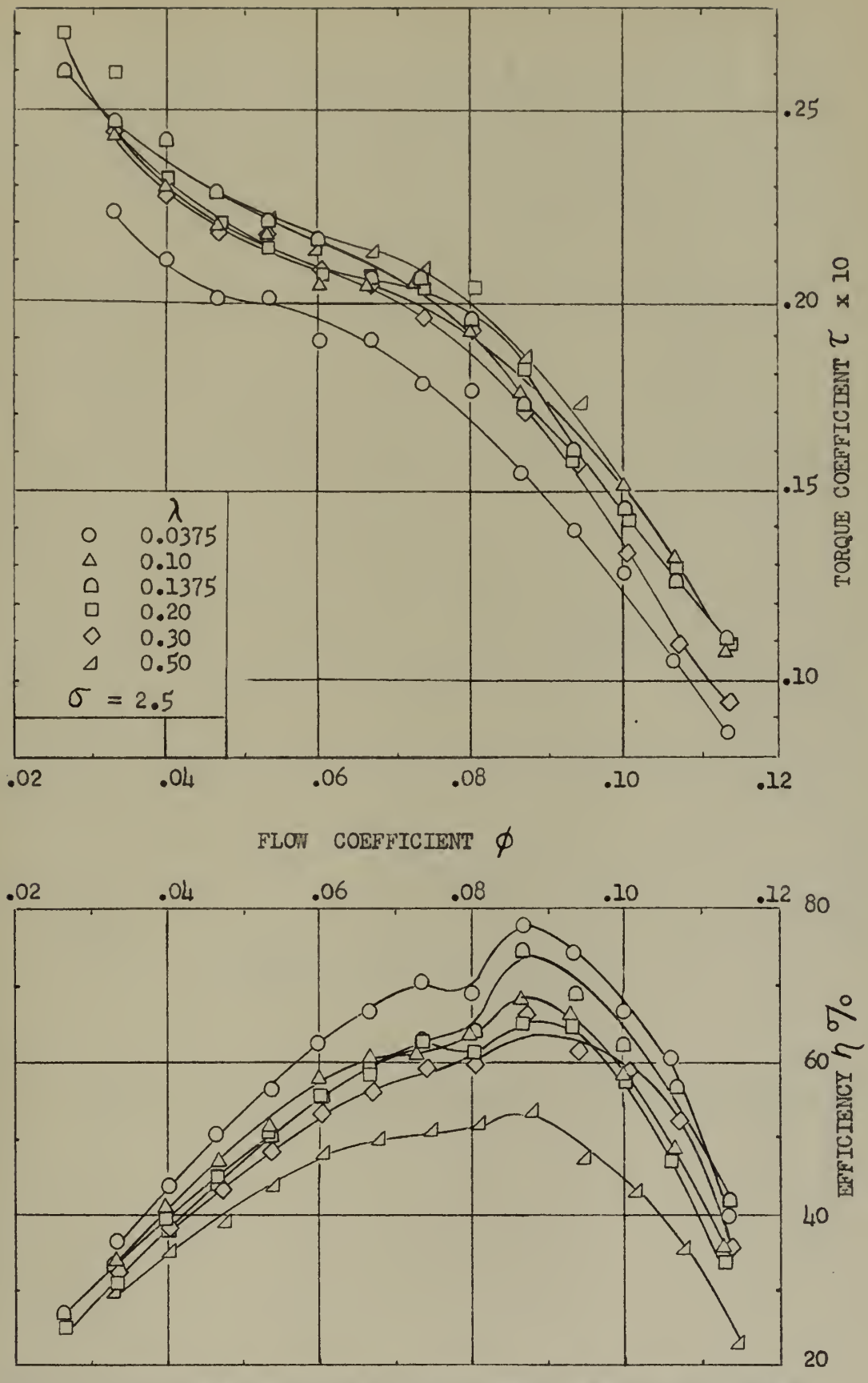

FIG. 7 TIP CLEARANCE EFFECT ON TORQUE COEFFICIENT AND EFFICIENCY

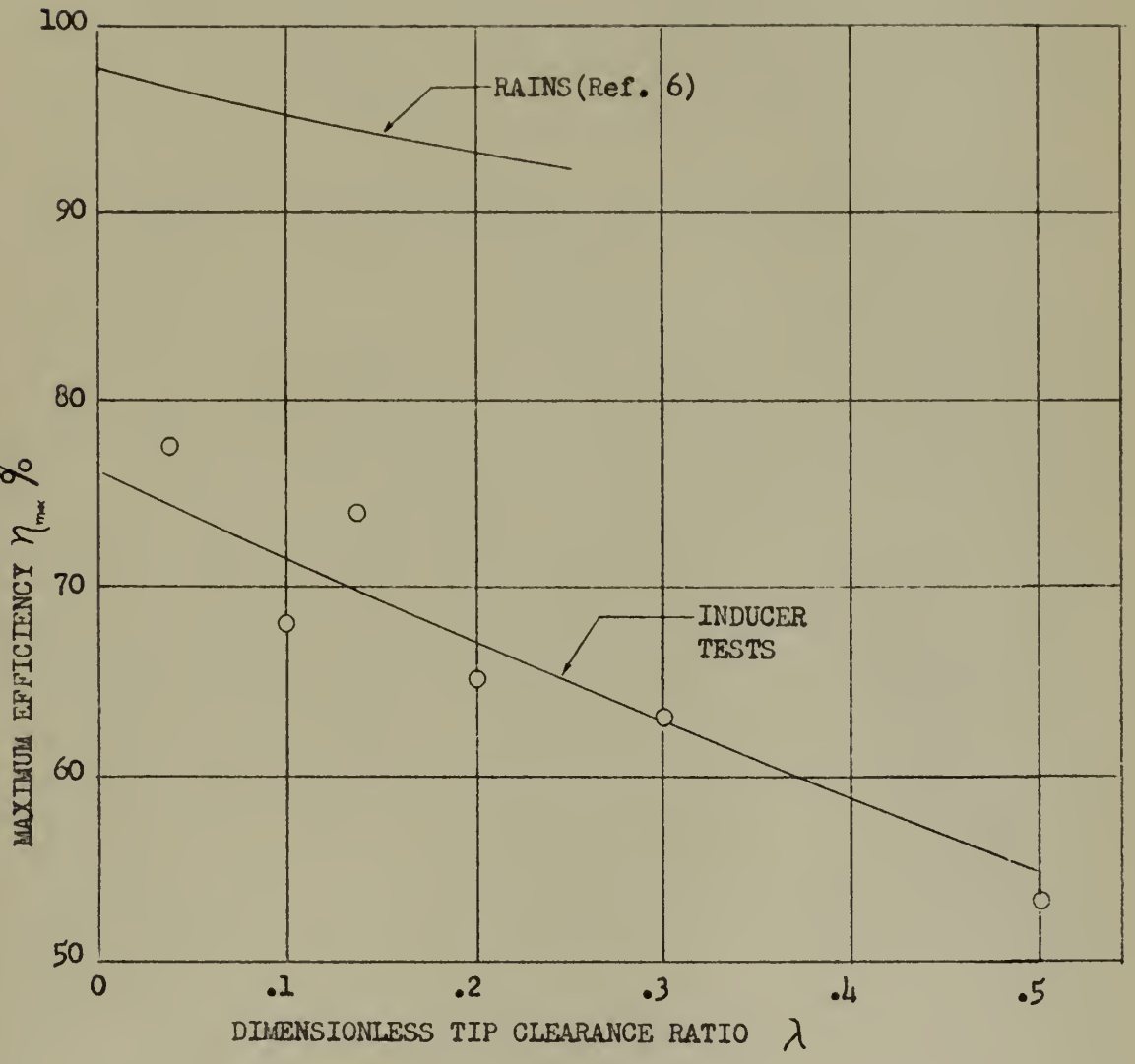

FIG. 8 MAXIMUM IMPELLER EFFICIENCY vs. TIP CLEARANCE RATIO, $\sigma = 2.5$

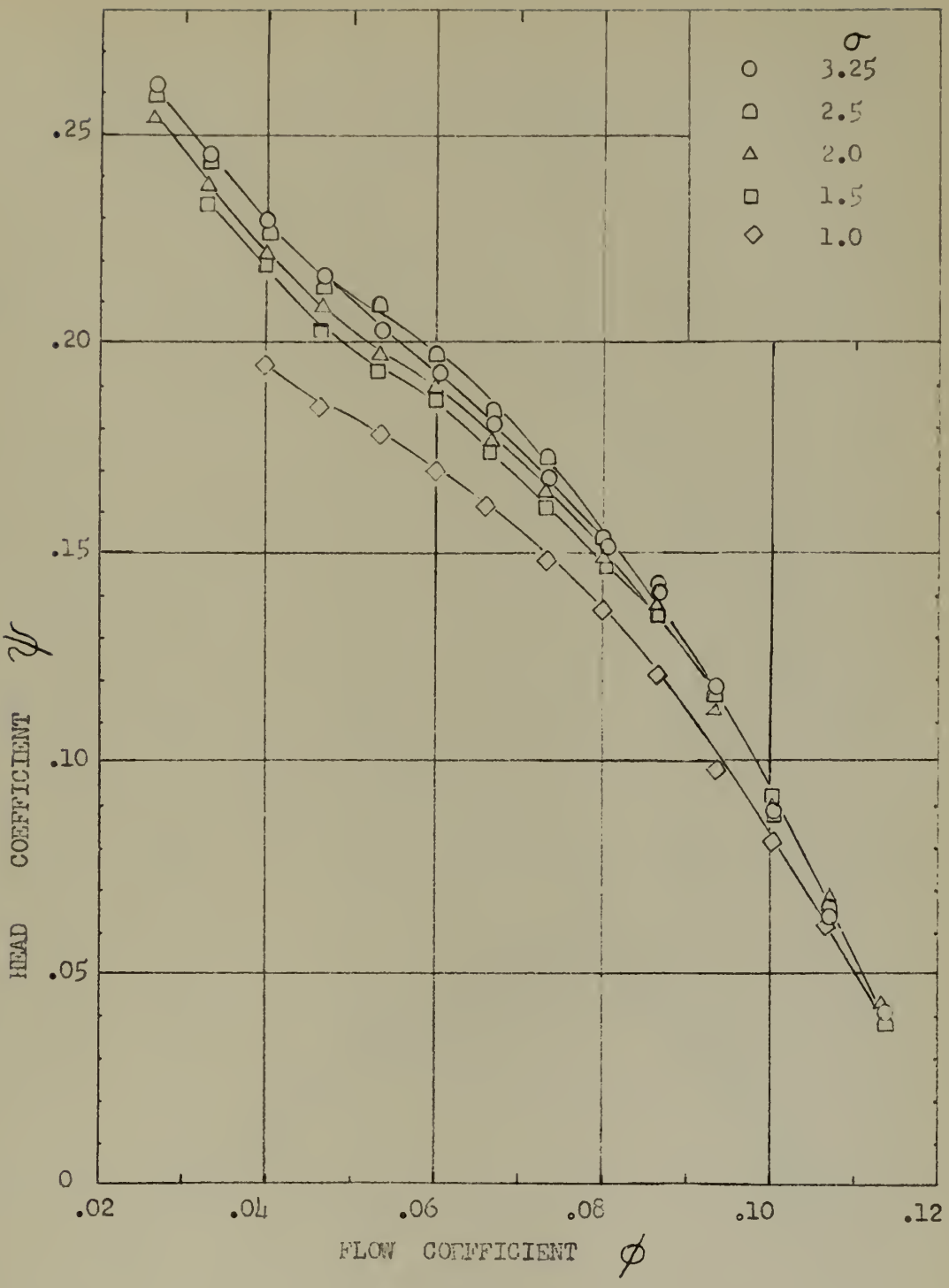

FIG. 9 HEAD COEFFICIENT vs. FLOW COEFFICIENT WITH VARYING SOLIDITY, $\lambda = 0.15$ EXCEPT FOR $\sigma = 2.5$ ($\lambda = 0.1375$)

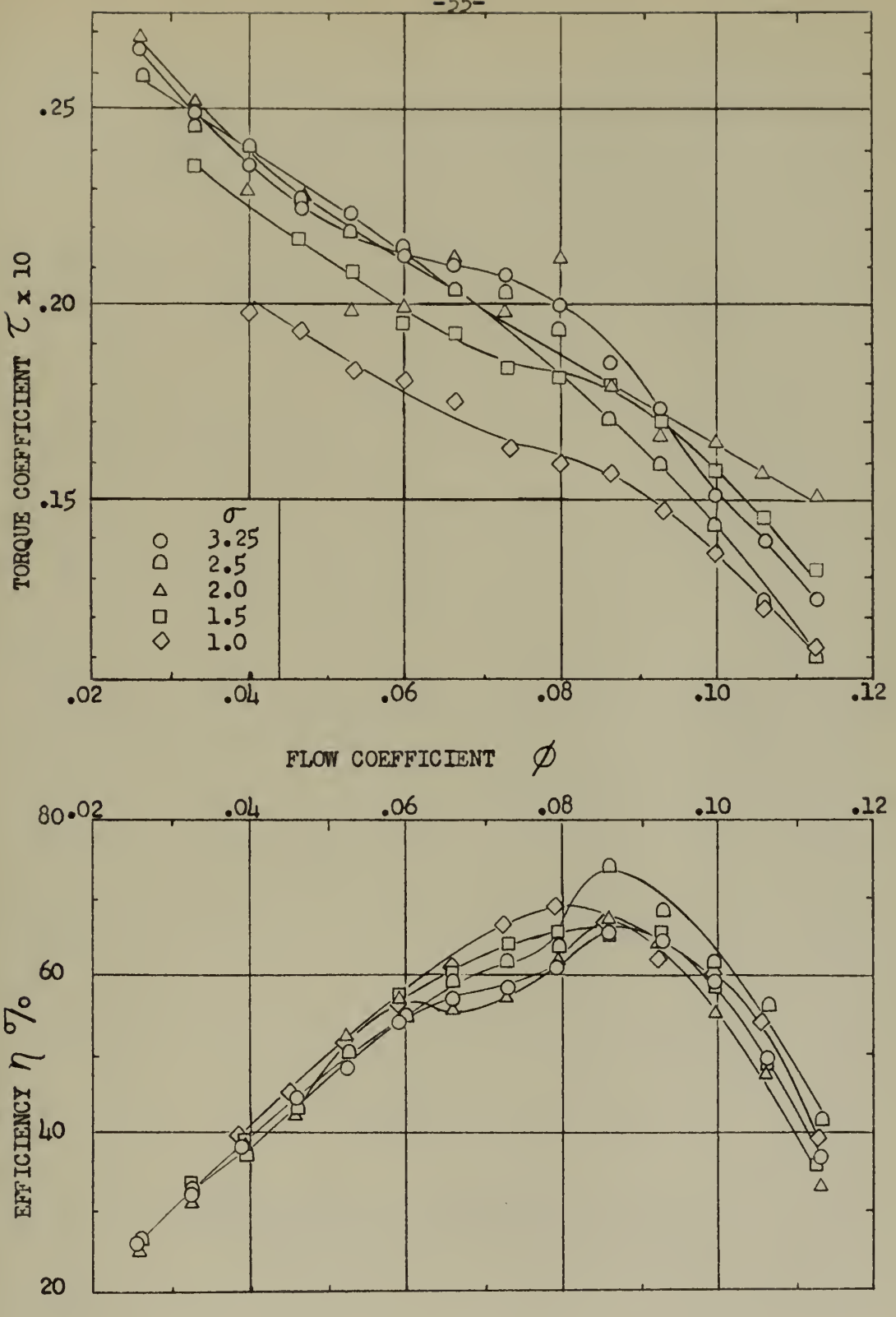

FIG. 10 TORQUE COEFFICIENT AND IMPELLER EFFICIENCY WITH VARYING SOLIDITY, $\lambda = 0.15$ EXCEPT FOR $\sigma = 2.5$ ($\lambda = 0.1375$)

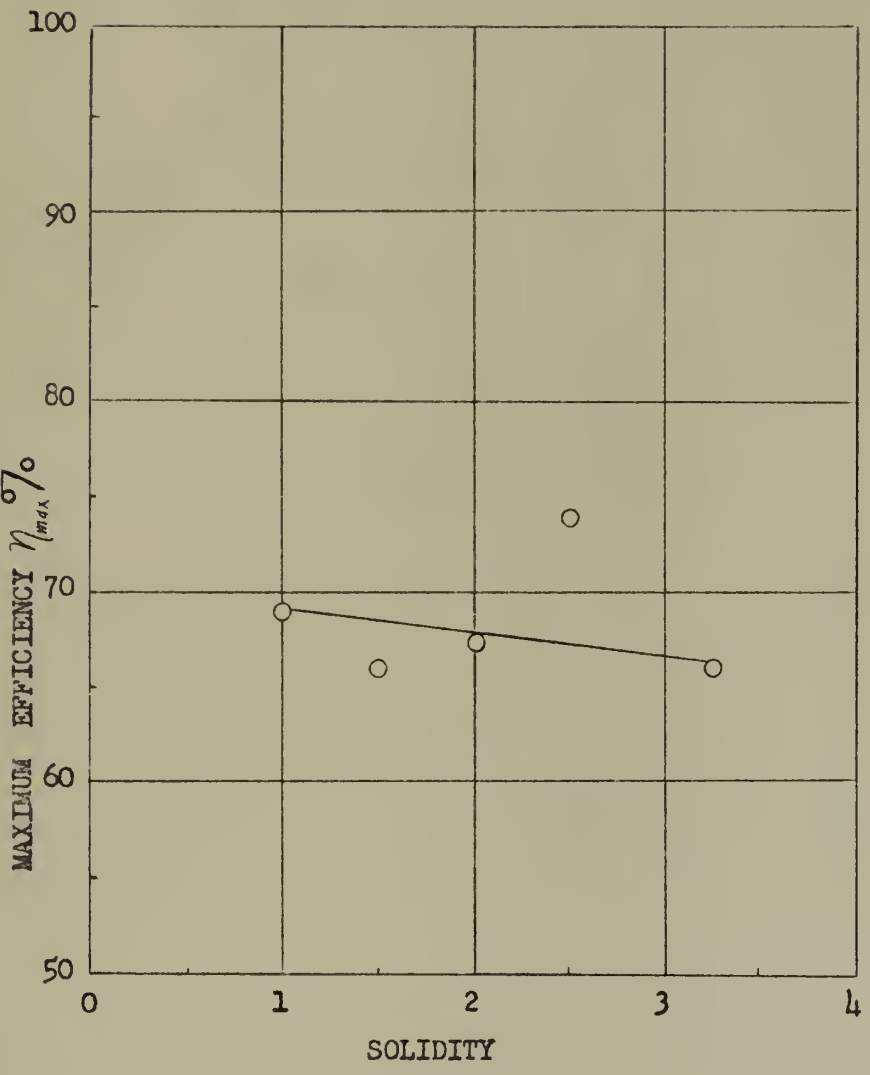

FIG. 11 MAXIMUM IMPELLER EFFICIENCY vs. SOLIDITY
λ = 0.15 EXCEPT FOR σ = 2.5 (λ = 0.1375)

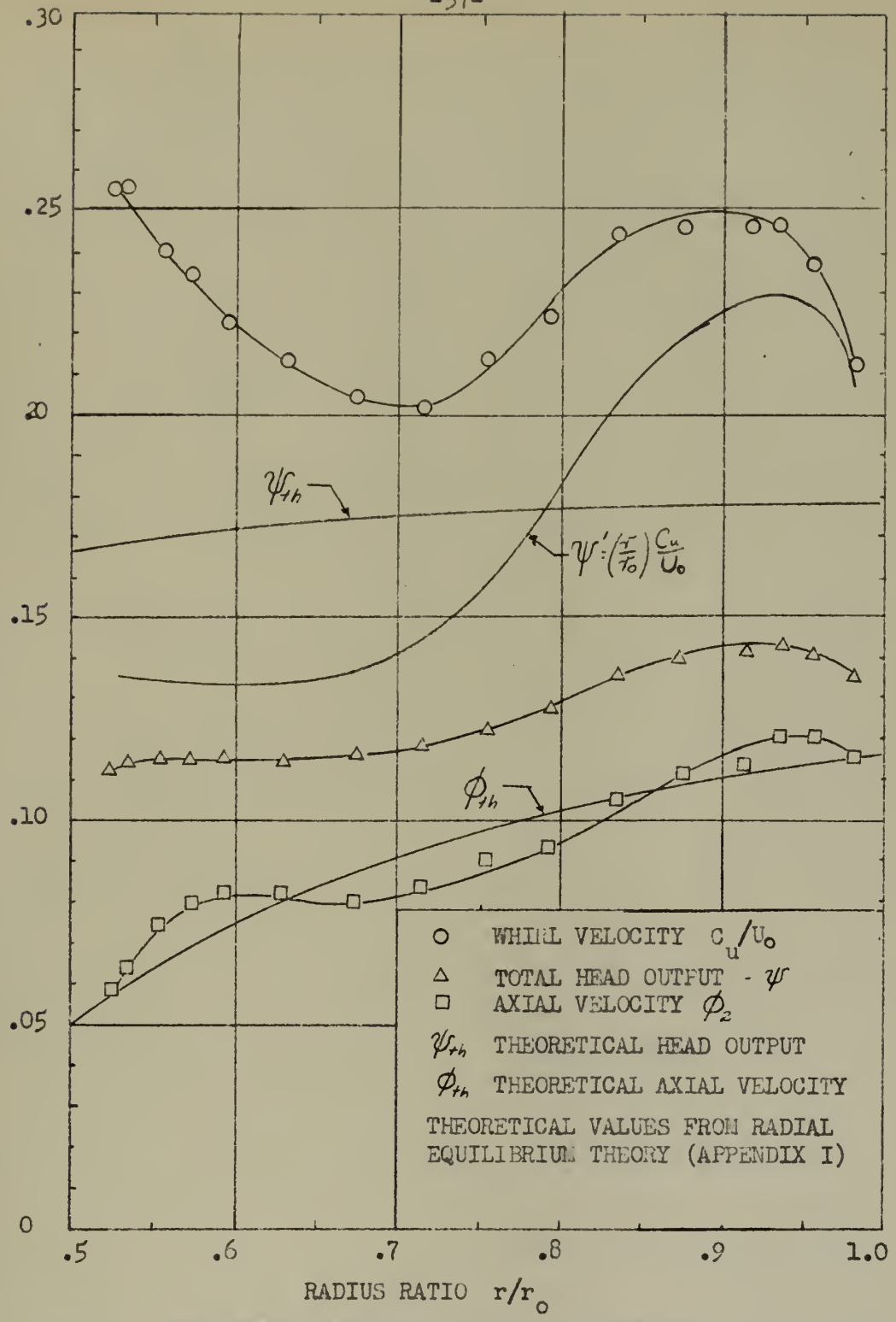

FIG. 12 COMPARISON OF THEORETICAL AND EXPERIMENTAL RADIAL HEAD AND VELOCITY DISTRIBUTIONS AT AN AVERAGE FLOW COEFFICIENT $\phi_1 = .093$ ($\lambda = .1375$, $\sigma = 2.5$)

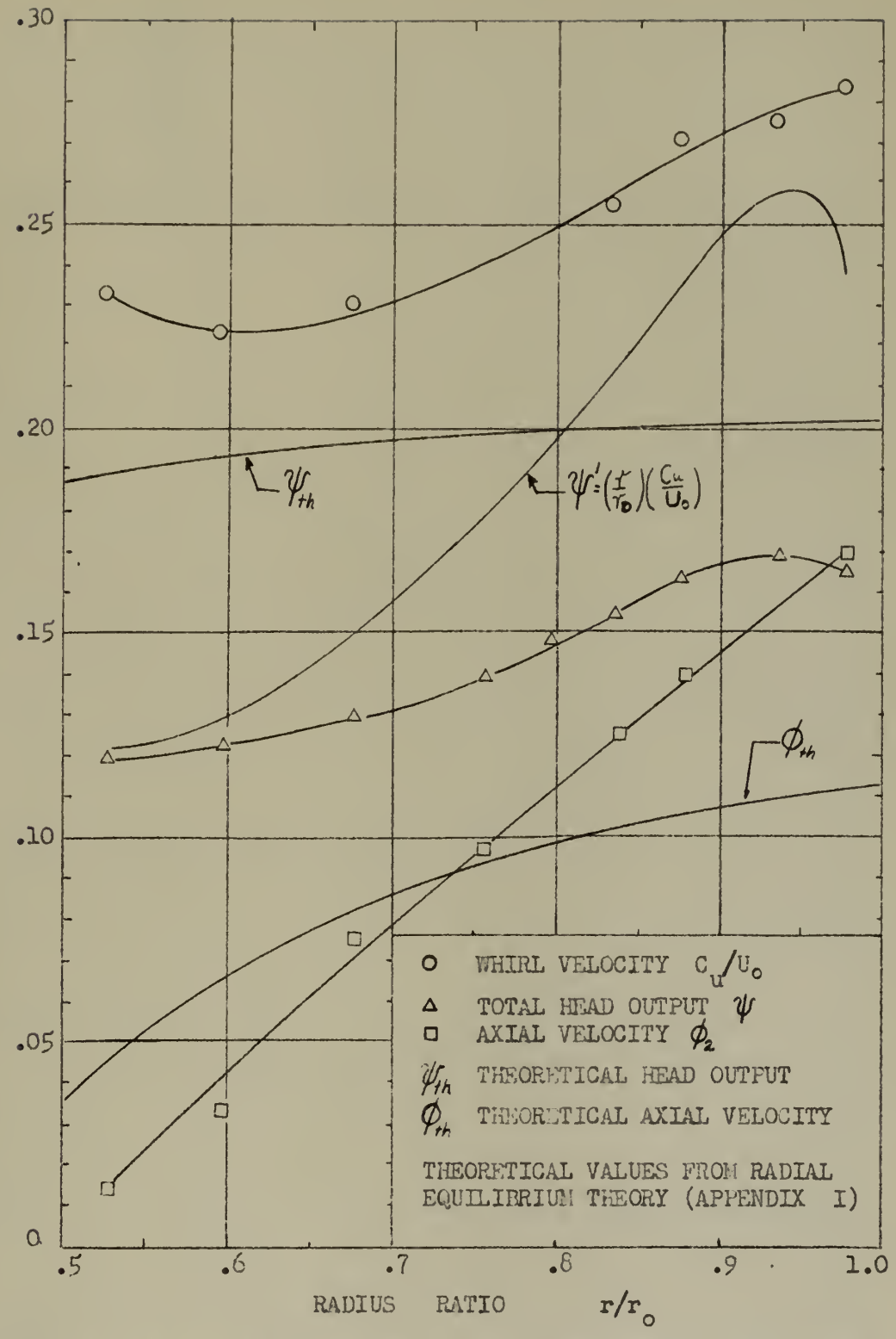

FIG. 13 COMPARISON OF THEORETICAL AND EXPERIMENTAL RADIAL HEAD AND VELOCITY DISTRIBUTIONS AT AN AVERAGE FLOW COEFFICIENT ϕ = .087 (λ = .1375, σ = 2.5)

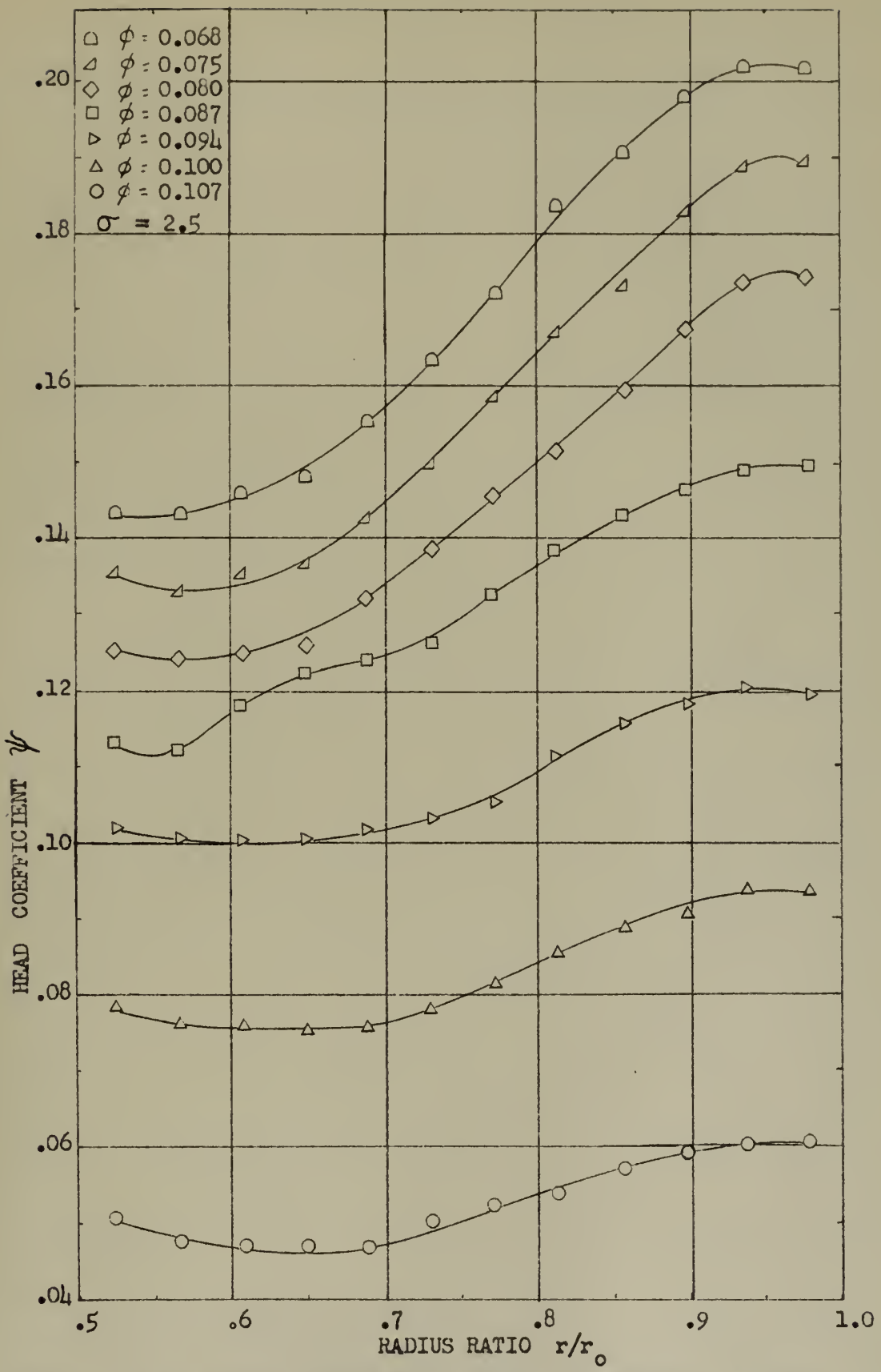

FIG. 14 RADIAL HEAD DISTRIBUTION - TYPICAL IMPELLER ($\lambda = .0375$)

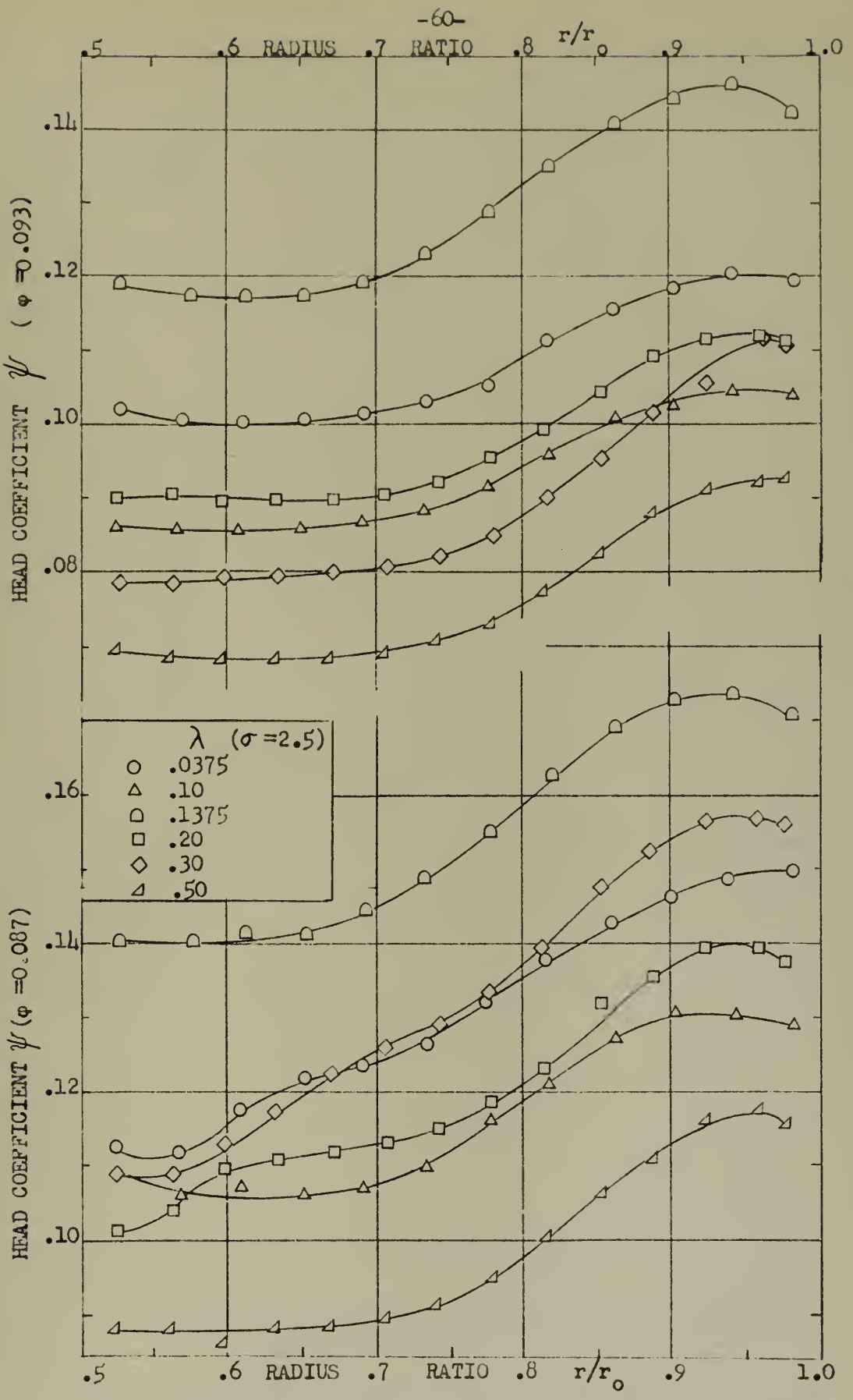

FIG. 15 EFFECT OF TIP CLEARANCE ON RADIAL HEAD DISTRIBUTION

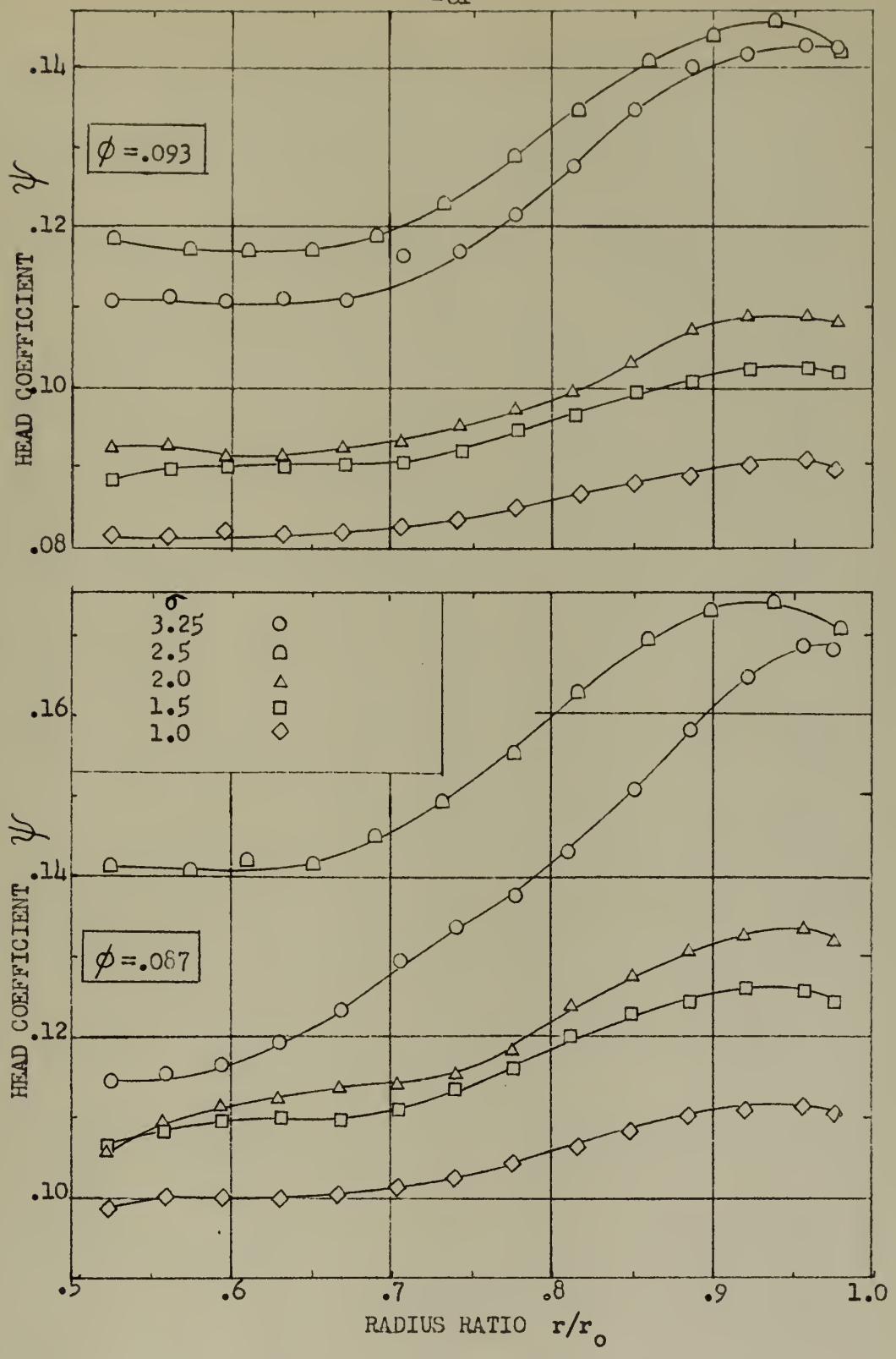

FIG. 16 EFFECT OF SOLIDITY ON RADIAL HEAD DISTRIBUTION
λ = 0.15 EXCEPT FOR σ = 2.5 (λ = 0.1375)

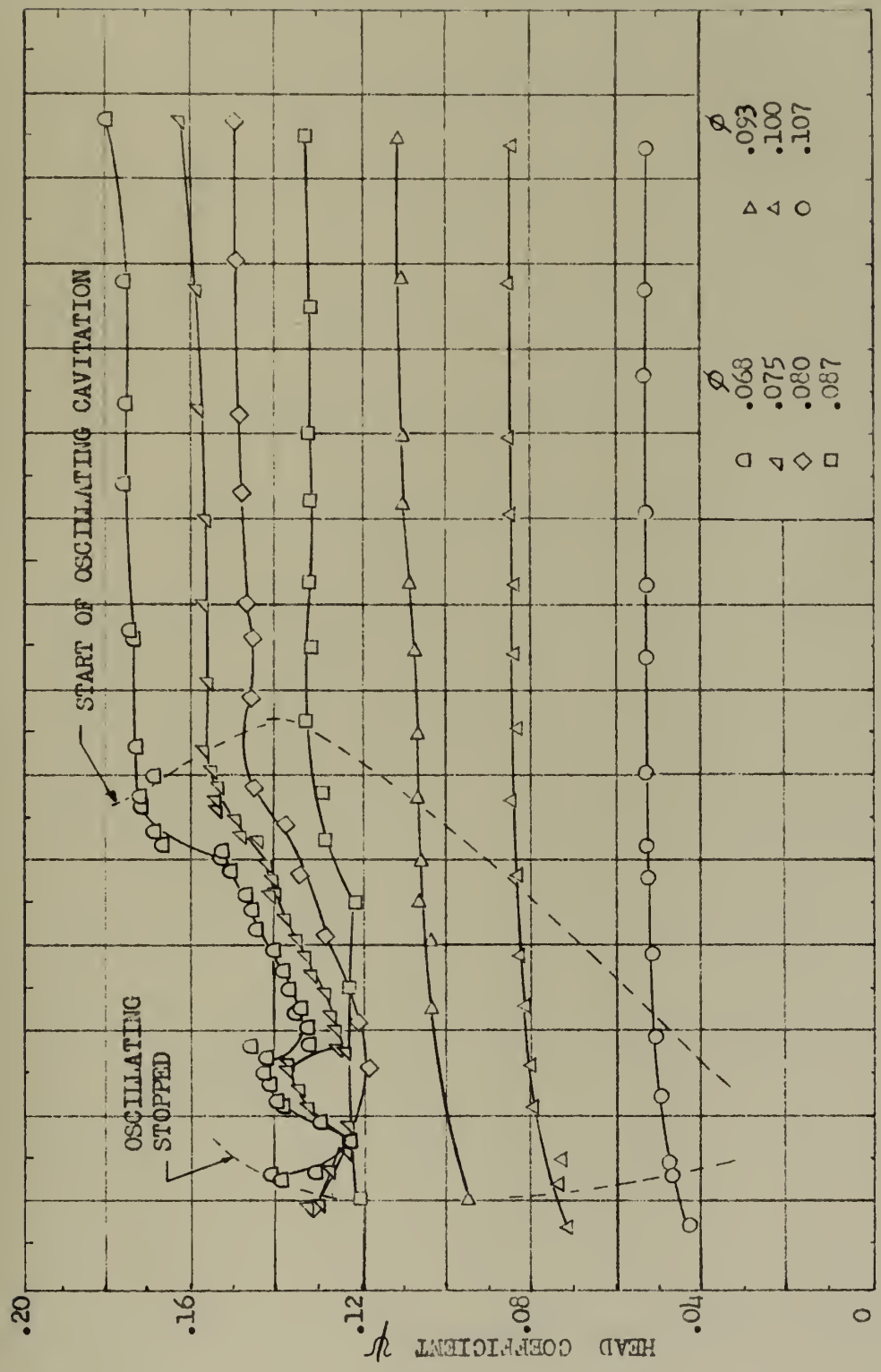

FIG. 17 CAVITATION NUMBER vs. HEAD COEFFICIENT FOR A TYPICAL IMPELLER ($\lambda = 0.0375, \sigma = 2.5$)

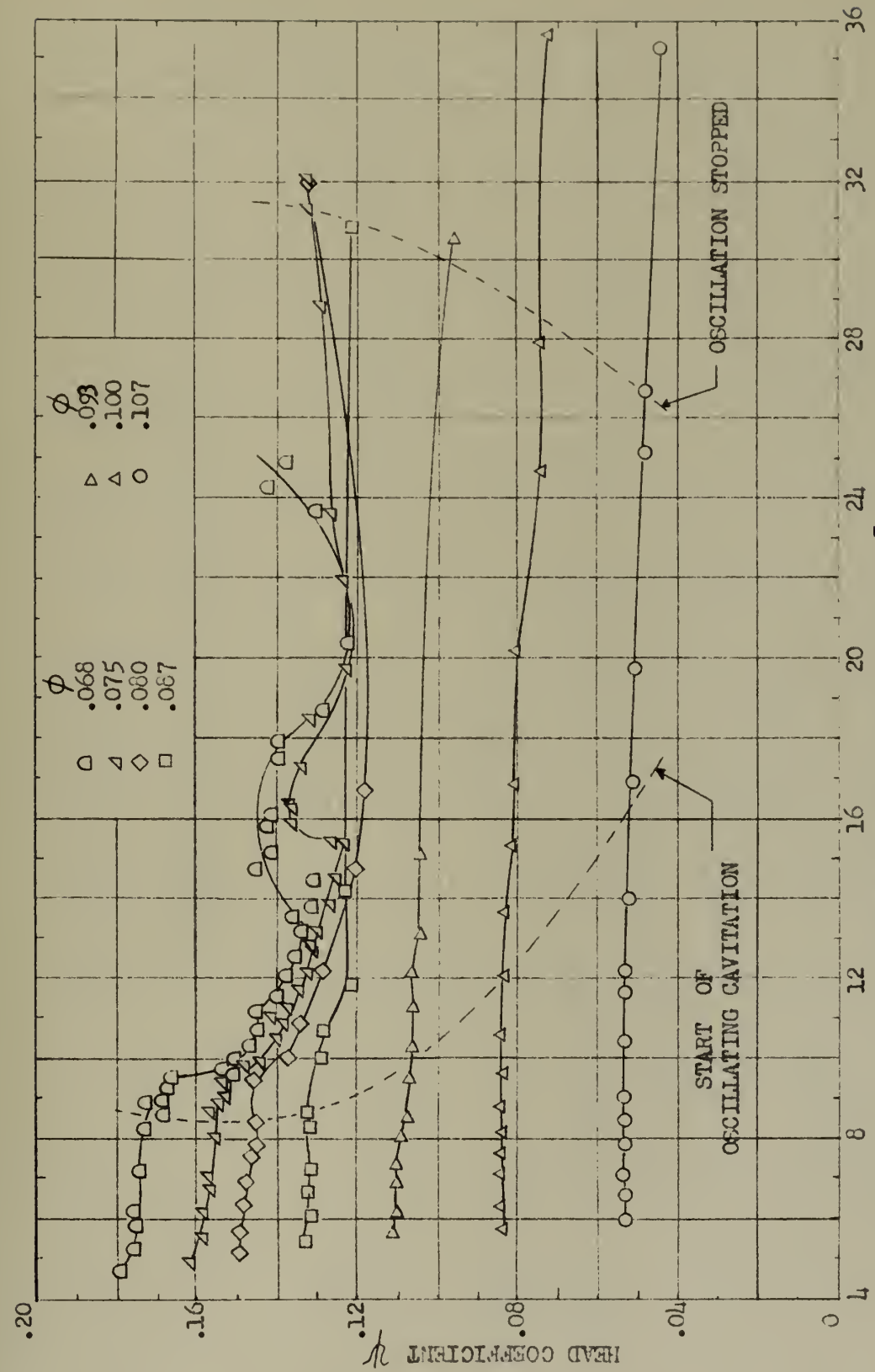

FIG. 18 SUCTION SPECIFIC SPEED vs. HEAD COEFFICIENT FOR A TYPICAL IMPELLER (λ = .0375, σ = 2.5)

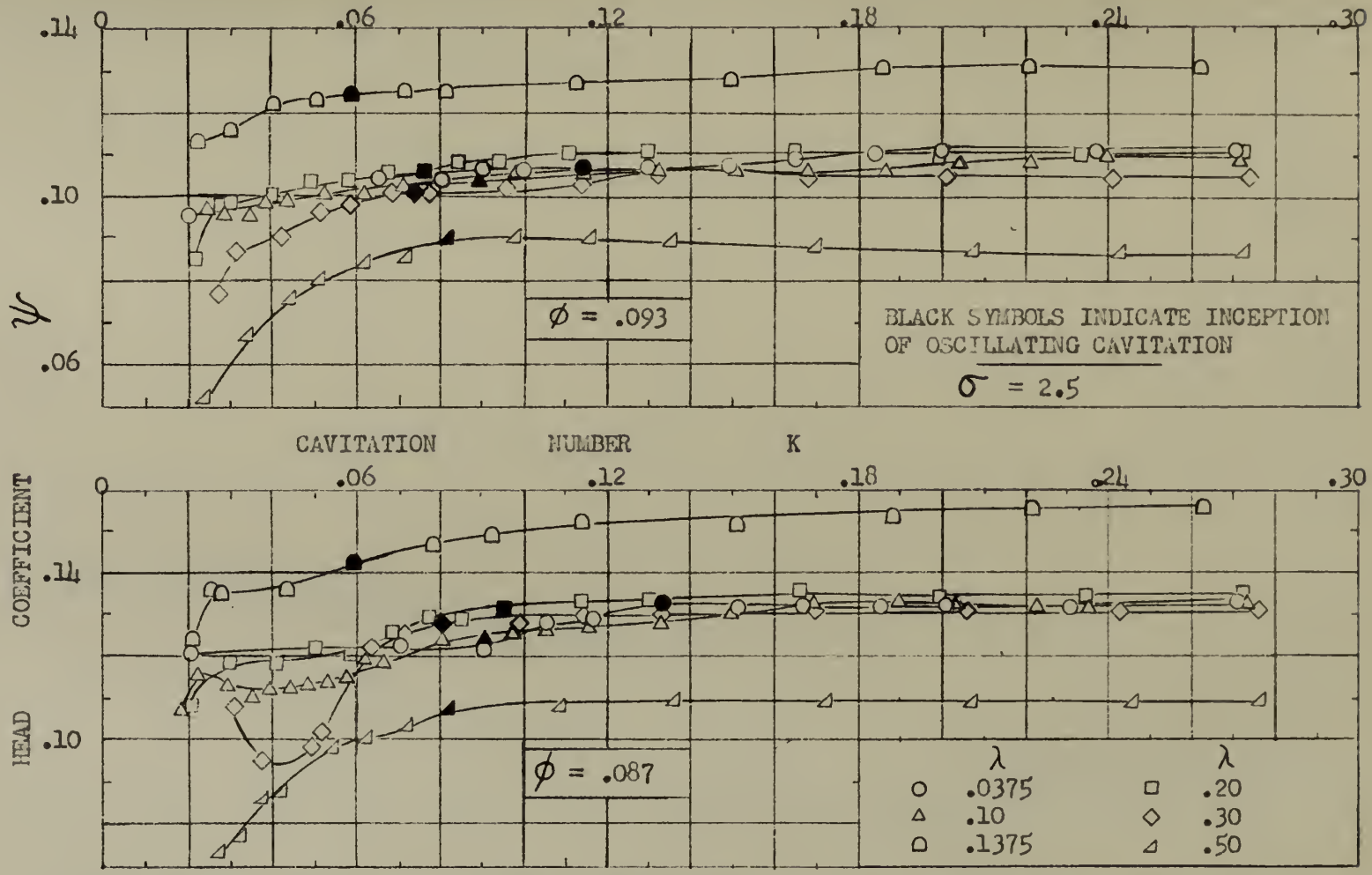

FIG. 19 EFFECT OF TIP CLEARANCE ON CAVITATING PERFORMANCE - CAVITATION NUMBER vs. HEAD COEFFICIENT

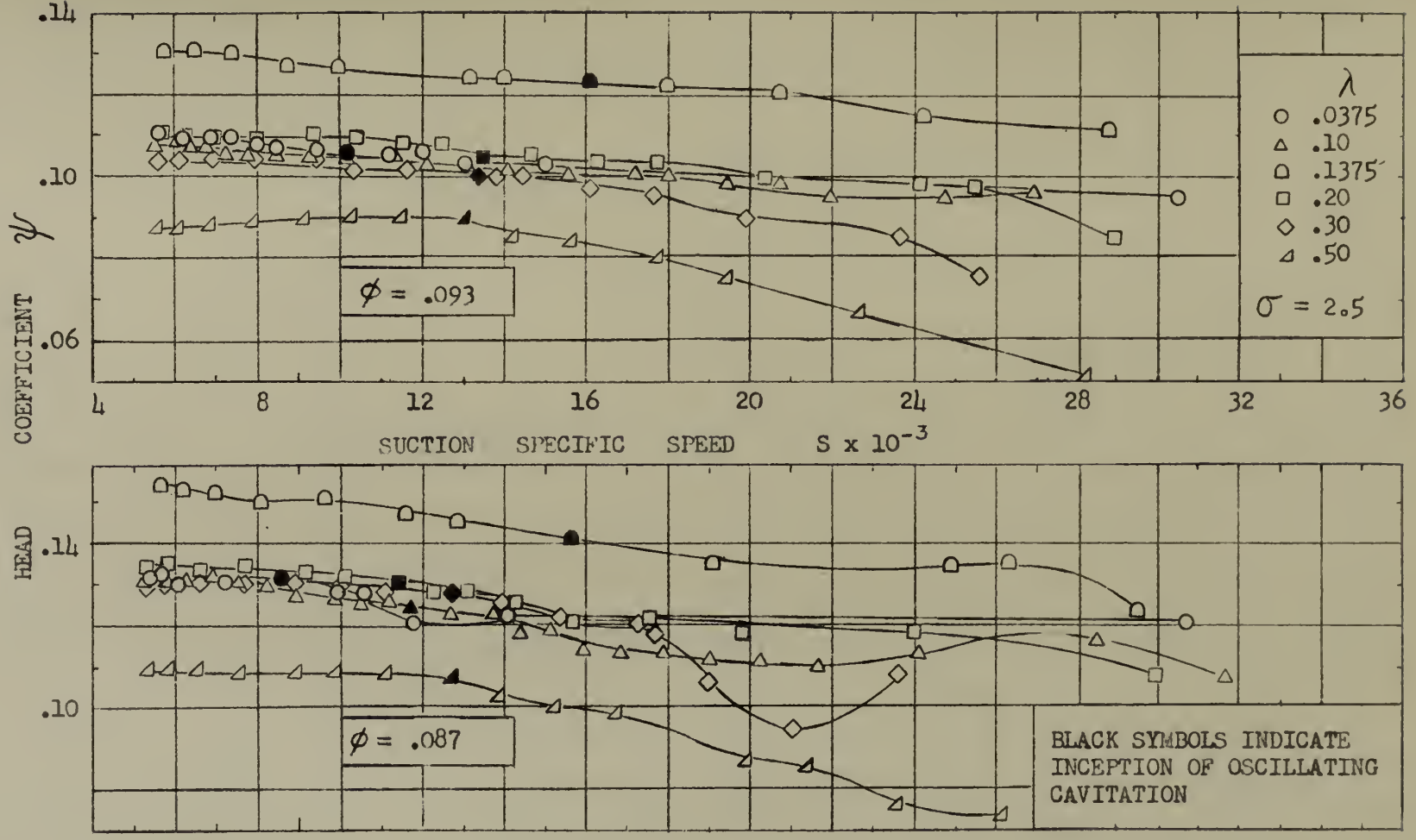

FIG. 20 EFFECT OF TIP CLEARANCE ON CAVITATING PERFORMANCE - SUCTION SPECIFIC SPEED vs. HEAD COEFFICIENT

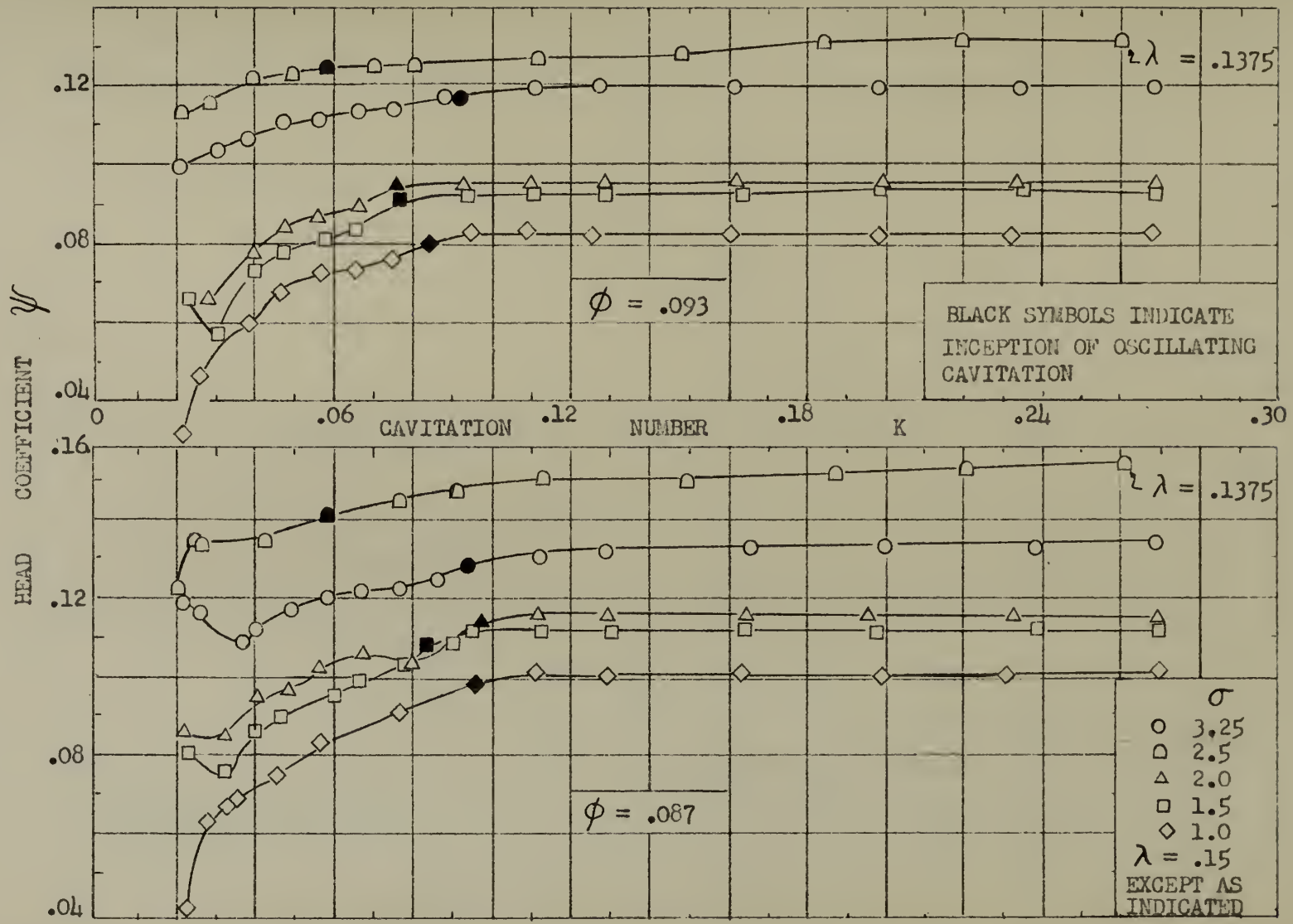

FIG. 21 EFFECT OF SOLIDITY ON CAVITATING PERFORMANCE - CAVITATION NUMBER vs. HEAD COEFFICIENT

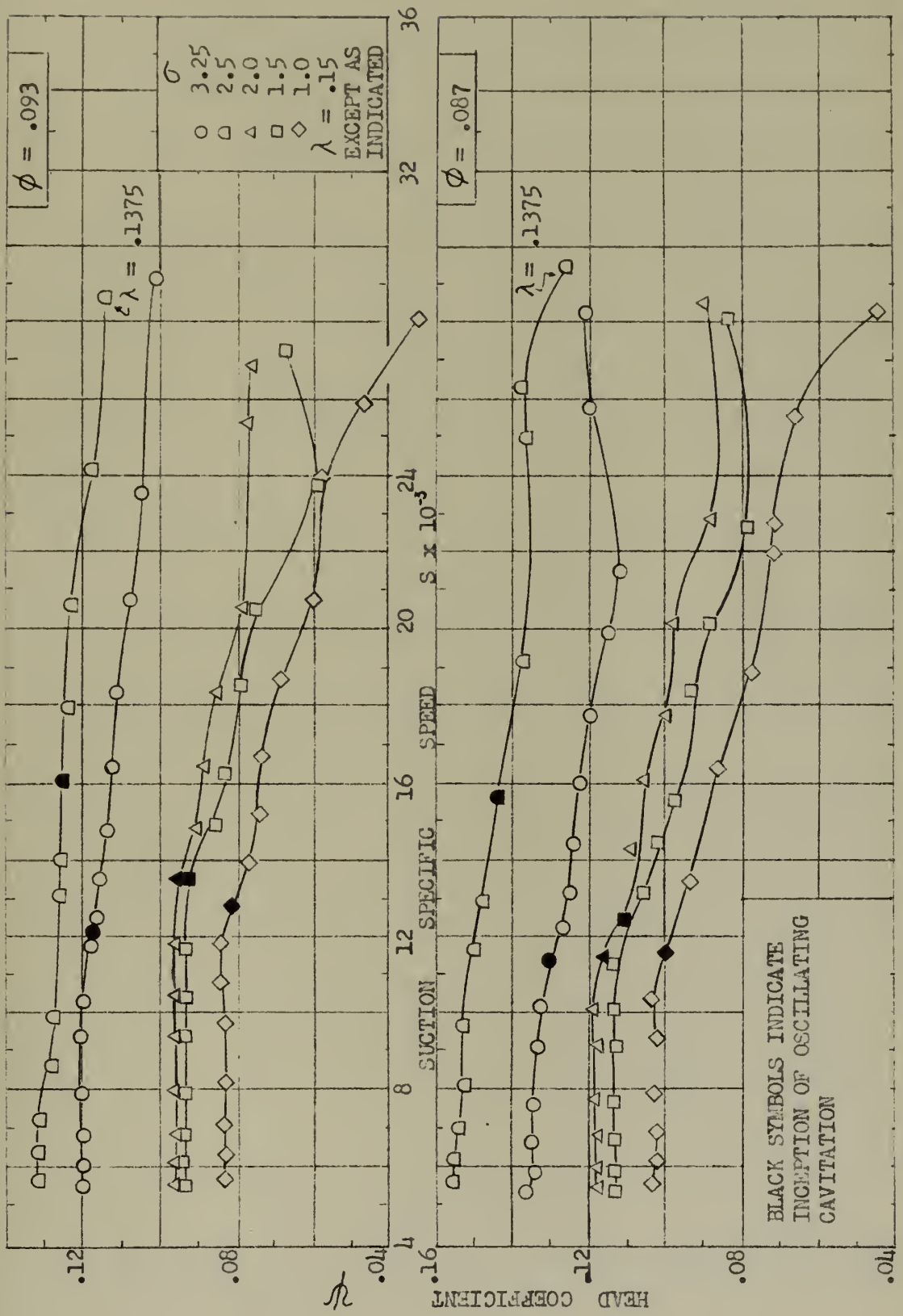

FIG. 22 EFFECT OF SOLIDITY ON CAVITATING PERFORMANCE - SUCTION SPECIFIC SPEED vs. HEAD COEFFICIENT

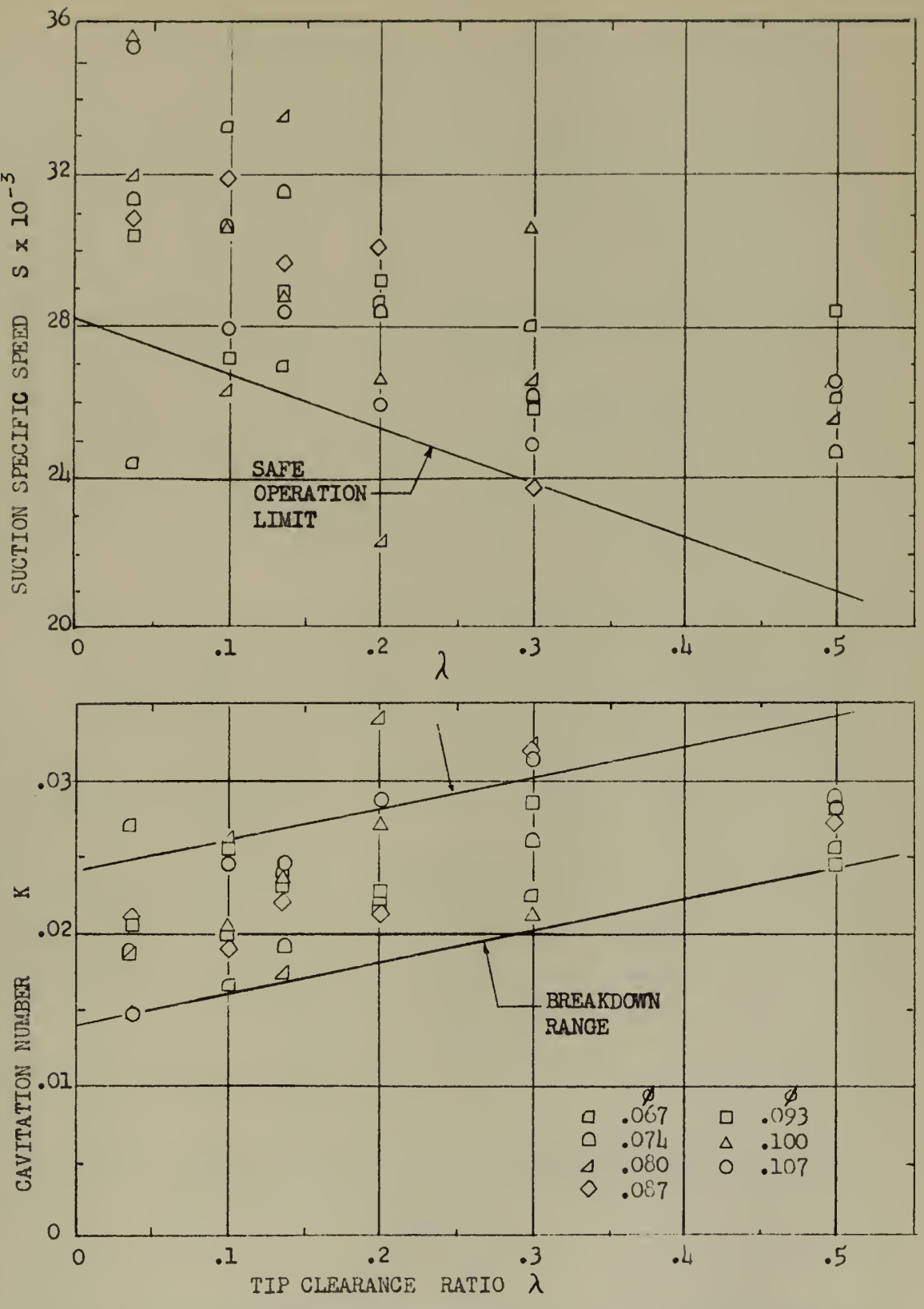

FIG. 23 SUCTION SPECIFIC SPEED AND CAVITATION NUMBER AT BREAKDOWN vs. TIP CLEARANCE RATIO, $\sigma = 2.5$

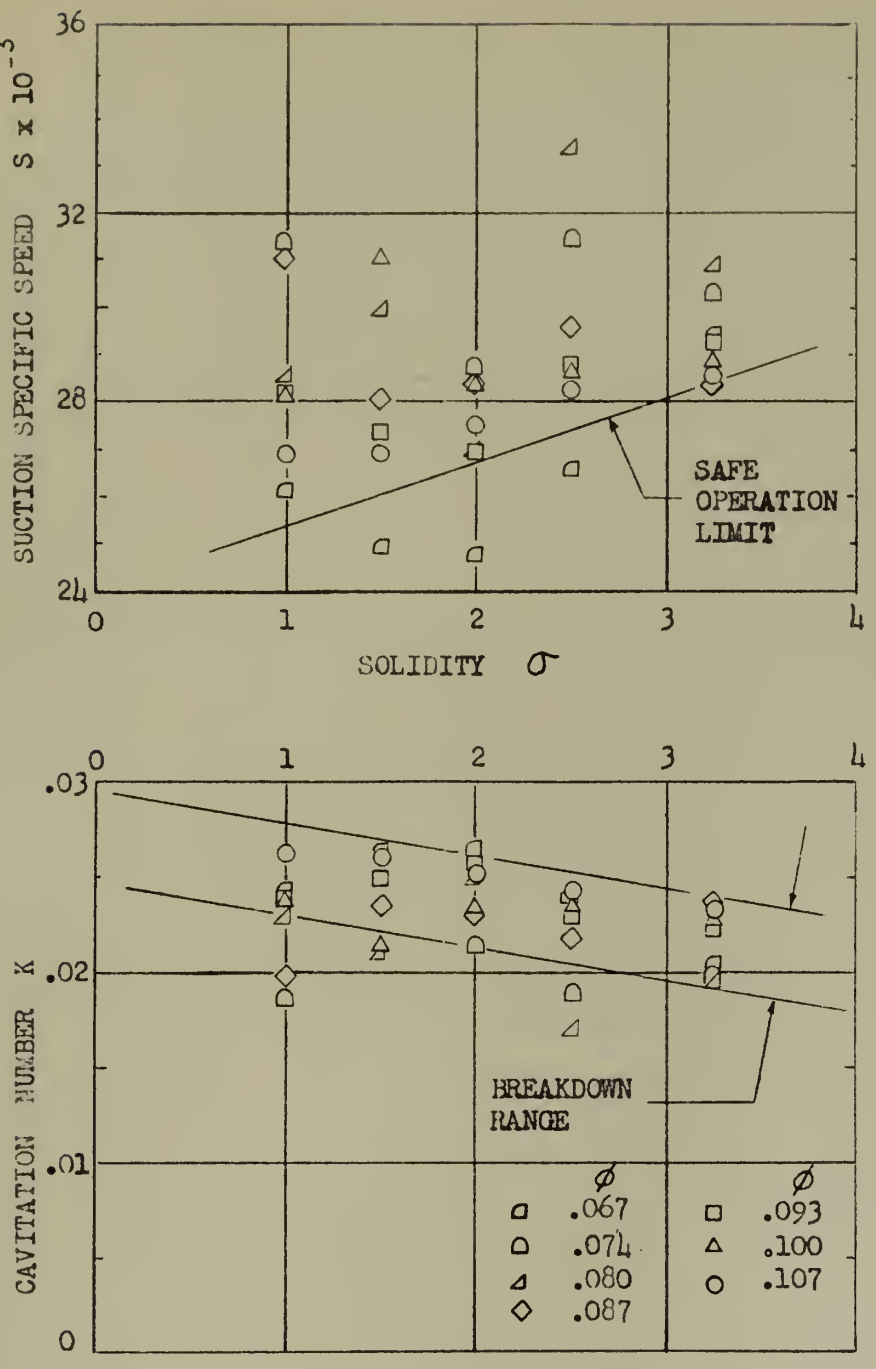

FIG. 24 SUCTION SPECIFIC SPEED AND CAVITATION NUMBER AT BREAKDOWN vs. SOLIDITY, $\lambda = 0.15$ EXCEPT FOR $\sigma = 2.5$ ($\lambda = 0.1375$)

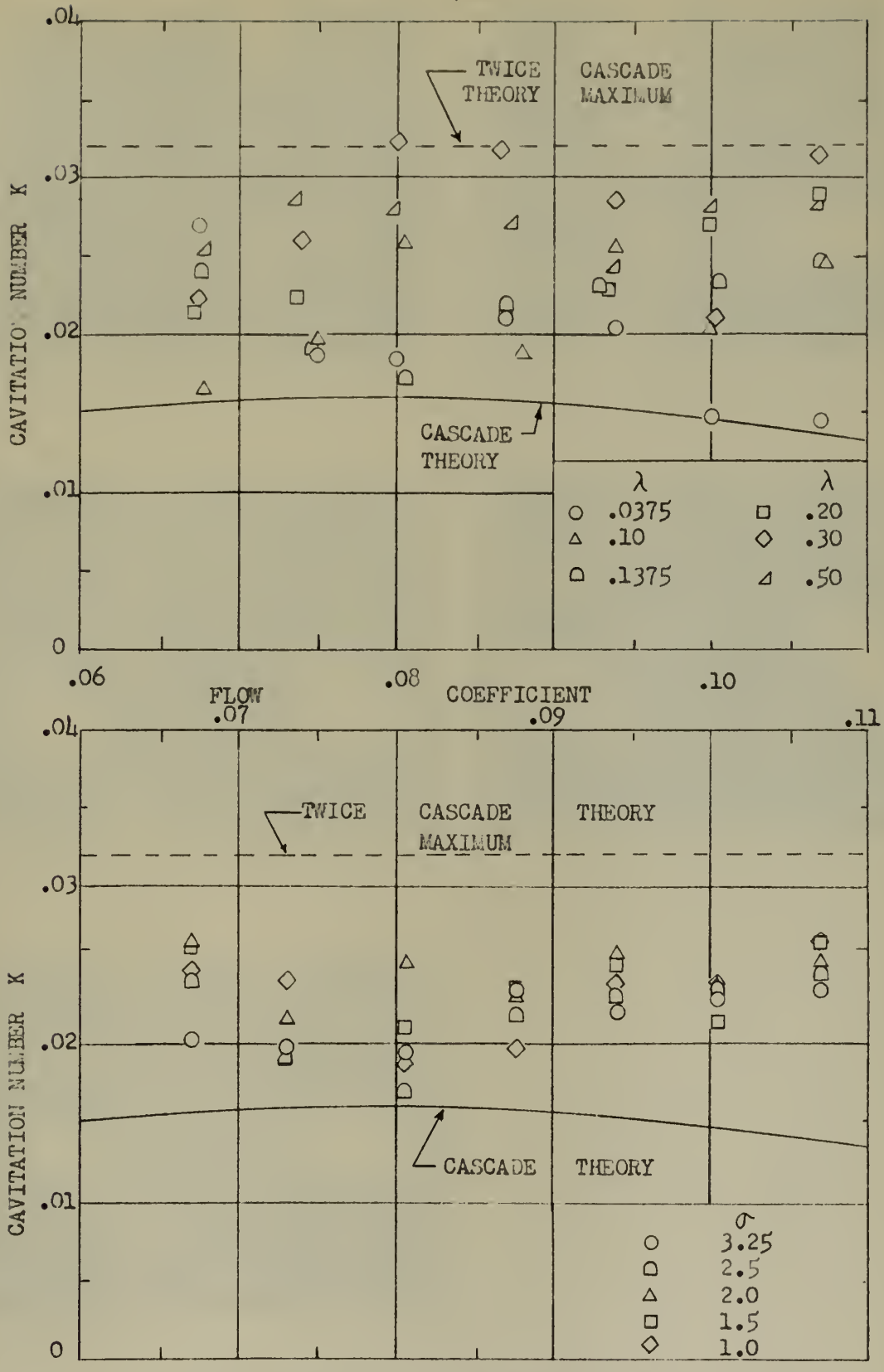

FIG. 25 CAVITATION NUMBER AT BREAKDOWN vs. FLOW COEFFICIENT with VARYING TIP CLEARANCE AND SOLIDITY

(a)

(b)

(c)

(d)

(e)

	K	S
(a)	0.2628	5,690
(b)	0.1151	9,680
(c)	0.0444	19,190
(d)	0.0264	26,410
(e)	0.0218	29,550

Fig.26 Cavitation Development, $\varphi = 0.087$, $\lambda = 0.1375$, $\sigma = 2.5$

λ = .0375 K = .1329 S = 8,714

λ = .100 K = .0870 S = 12,225

λ = .1375 K = .0604 S = 15,690

λ = .200 K = .0814 S = 12,840

λ = .300 K = .0799 S = 13,028

λ = .500 K = .0837 S = 12,759

Fig. 27 Start of Oscillating Cavitation, $\varphi = 0.087$, λ varying

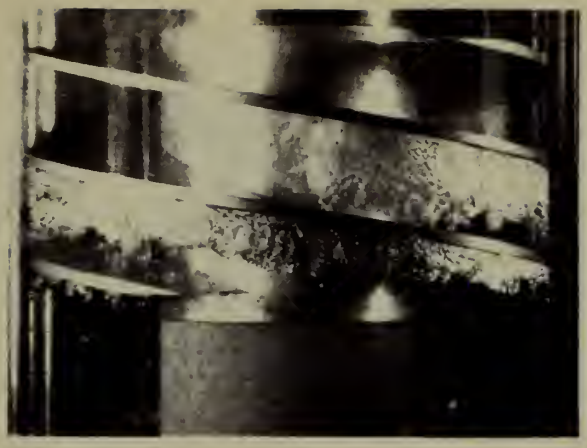

λ = .0375 K = .0242 S = 26,849

λ = .100 K = .0220 S = 28,506

λ = .1375 K = .0190 S = 31,468

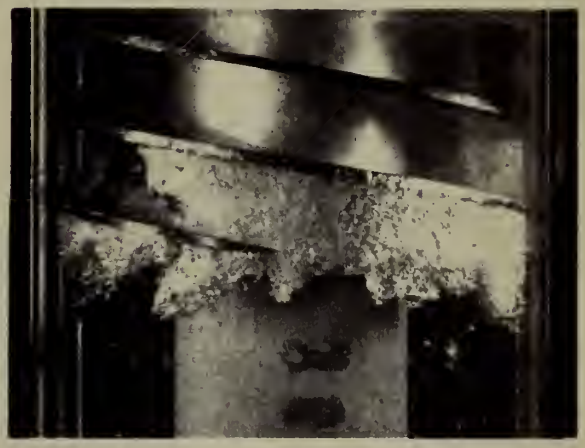

λ = .200 K = .0262 S = 25,668

λ = .300 K = .0207 S = 29,771

λ = .500 K = .0267 S = 25,772

Fig.28 Appearance Near Breakdown, φ = 0.074, λ varying

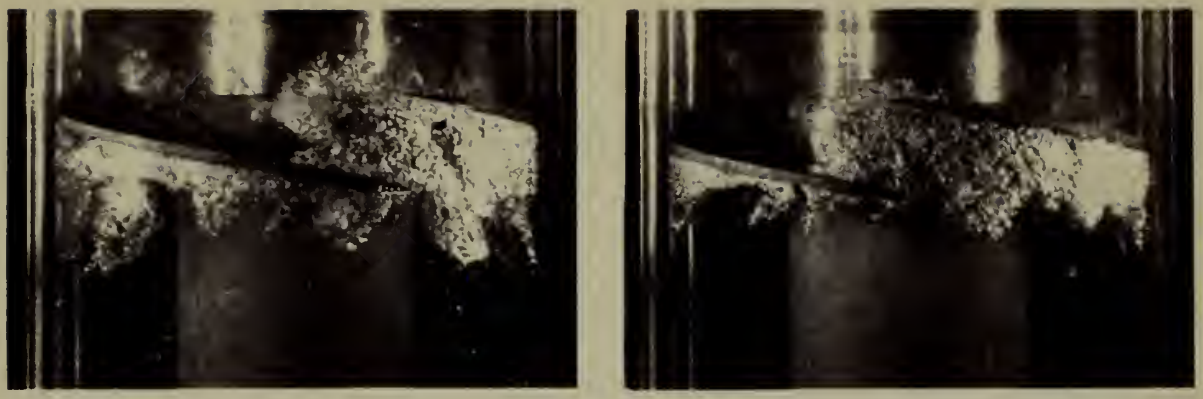

φ = .087 K = .0357 S = 21,941 φ = .073 K = .0320 S = 22,544

Fig. 29 Backflow at Trailing Edge During Oscillating Cavitation, σ = 1.0

Fig. 30 Appearance of Suction Surface Near Breakdown, φ = .107, λ = .0375, K = .0277, S = 26,192. Direction of rotation is to left (in all other photographs rotation is to right).